HHS Public Access

Author manuscript

Neurobiol Dis. Author manuscript; available in PMC 2020 July 01.

Published in final edited form as:

Neurobiol Dis. 2019 July ; 127: 527–544. doi:10.1016/j.nbd.2019.03.024.

The UPR-PERK pathway is not a promising therapeutic target for mutant SOD1-induced ALS

Yulia Dzhashiashvili, **Chase P. Monckton**[1], **Harini S. Shah**, **Rejani B. Kunjamma**, and **Brian Popko**[*]

Department of Neurology, The University of Chicago Center for Peripheral Neuropathy, The University of Chicago, Chicago, Illinois, 60637

Abstract

Amyotrophic lateral sclerosis (ALS) is a progressive neurodegenerative disease, characterized by motor neuron death in the brain and spinal cord. Mutations in the Cu/Zn superoxide dismutase (*SOD1*) gene account for ~20% of all familial ALS forms, corresponding to 1%–2% of all ALS cases. One of the suggested mechanisms by which mutant SOD1 (mtSOD1) exerts its toxic effects involves intracellular accumulation of abnormal mtSOD1 aggregates, which trigger endoplasmic reticulum (ER) stress and activate its adaptive signal transduction pathways, including the unfolded protein response (UPR). PERK, an eIF2α kinase, is central to the UPR and is the most rapidly activated pathway in response to ER stress. Previous reports using mtSOD1 transgenic mice indicated that genetic or pharmacological enhancement of the UPR- PERK pathway may be effective in treating ALS. We investigated the response to *PERK* haploinsufficiency, and the response to deficiency of its downstream effectors *GADD34* and *CHOP*, in five distinct lines of mtSOD1 mice. We demonstrate that, in contrast to a previously published study, *PERK* haploinsufficiency has no effect on disease in all mtSOD1 strains examined. We also show that deficiency of *GADD34*, which enhances the UPR by prolonging the phosphorylation of eIF2α does not ameliorate disease in these mtSOD1 mouse strains. Finally, we demonstrate that genetic ablation of *CHOP* transcription factor, which is known to be pro-apoptotic, does not ameliorate disease in mtSOD1 mice. Cumulatively, our studies reveal that neither genetic inhibition of the UPR via ablation of *PERK*, nor genetic UPR enhancement via ablation of *GADD34*, is beneficial for mtSOD1-induced motor neuron disease. Therefore, the PERK pathway is not a likely target for therapeutic intervention in ALS.

[*]Corresponding author at: The University of Chicago, Department of Neurology, MC2030, 5841 S. Maryland Ave.Chicago, IL 60637. bpopko@uchicago.edu.

1 Present address: Department of Bioengineering, University of Illinois at Chicago, Chicago, Illinois, 60607.

Author contributions

YD designed research, performed research and analyzed data. CM, HS and RK performed research. BP conceived and coordinated the study. YD and BP wrote the paper. All authors read and approved the final paper.

Declarations of interest

The authors declare no conflict of interest.

Materials and Data Availability

All data are available upon reasonable request to the corresponding author.

Keywords

Amyotrophic lateral sclerosis; SOD1 mice; motor neurons; endoplasmic reticulum stress; unfolded protein response; PERK; GADD34; CHOP

Introduction

Amyotrophic lateral sclerosis (ALS) is a late-onset progressive neurodegenerative disease that is characterized by the selective loss of motor neurons. It leads to paralysis and ultimately death due to respiratory failure, typically within several years after onset (1–4). Most cases of ALS (90%) are without an obvious genetic component (sporadic), whereas approximately 10% are inherited in a dominant manner (familial). Since sporadic and familial forms of ALS are clinically similar, understanding the mechanisms underlying familial ALS may provide insights into both forms of the disease. Although it is unclear what causes motor neuron demise in ALS, studies conducted using spinal cord samples from sporadic ALS patients and transgenic mouse models of familial ALS detected endoplasmic reticulum (ER) stress in both forms of the disease, suggesting that the ER stress response plays an important role in ALS pathogenesis (5–10). Notably, motor neurons are thought to be particularly vulnerable to ER stress in part due to their intrinsically low expression of ER chaperones (11). Mutant superoxide dismutase SOD1 (mtSOD1) induces cell-autonomous and non-cell autonomous motor neuron death through a toxic gain of function (12–14). One of the proposed toxicities involves accumulation of intracellular SOD1 aggregates, which may trigger ER stress and activate adaptive signal transduction pathways, including the unfolded protein response (UPR). The guiding hypothesis is that the toxicity of mtSOD1 arises from its ability to inhibit ER-associated degradation machinery, which is involved in export of misfolded proteins from the ER to the ubiquitin proteasome system, via binding to the integral membrane protein Derlin-1 (15, 16).

The PERK (protein kinase RNA-activated (PKR)-like ER kinase, encoded by *Eif2ak3*) pathway is one of the three principal signaling branches of the UPR and is the most rapidly activated pathway triggered by the presence of mis- or unfolded proteins in the ER (17–19). It is also central to the integrated stress response (ISR), which is activated by phosphorylation of eIF2α (eukaryotic translation initiation factor 2α) by a family of protein kinases in response to cellular stresses (20). The active (phosphorylated) form of PERK directly phosphorylates eIF2α, which leads to the reduction of global protein synthesis. The resulting effect is prevention of protein overload in the ER. At the same time, there is a preferential translation of ATF4 (activating transcription factor 4), which induces the expression of cytoprotective genes whose functions are to restore proteostasis. One of these genes, *Ppp1r15a*, encodes GADD34 (growth arrest and DNA damage-inducible 34), which acts in a feedback loop to dephosphorylate p-eIF2α and restore general protein synthesis. Under conditions of chronic stress, however, the PERK-ATF4 axis positively regulates CHOP (C/EBP homologous protein, encoded by *Ddit3*), one of the key pro-apoptotic players in the UPR (21). Murine mouse models to study the UPR, including mice genetically deficient for *PERK*, *GADD34*, and *CHOP*, have been invaluable in understanding the contribution of the UPR during stress conditions (22).

Studies using genetic or pharmacological approaches to manipulate the UPR have revealed the potential involvement of PERK signaling in mtSOD1-induced ALS (23, 24). *PERK* haploinsufficiency accelerated the accumulation of misfolded SOD1 and shortened life span in *G85R* mice (25), and *GADD34* haploinsufficiency was shown to protect *G85R* mice against the disease (26). Pharmacological modulation of GADD34 has been accomplished in *G93A* high- copy (*G93A*-HC) mice using several small molecule inhibitors: salubrinal, guanabenz, and Sephin1. These studies demonstrated a protective effect of blocking GADD34 activity, which results in a prolonged ER stress response (9, 27–29), with an exception of one report, where guanabenz was shown to exacerbate disease (30). In comparison, little is known regarding the role of CHOP in ALS. Although increased CHOP expression has been detected in spinal cords of sporadic ALS patients and familial ALS mouse models (5, 31), the significance of these findings to ALS pathogenesis remains uncertain.

Considering the contradictory evidence regarding the protective effects of the UPR in experimental models of ALS, the contribution of the PERK pathway to ALS needs to be better defined. Using a genetic approach in several well-characterized mtSOD1 mouse models (Table 1), we demonstrate that neither diminished, nor enhanced, UPR capacity significantly affect the disease. These results were consistent across all five mtSOD1 mouse models studied. Therefore, the PERK pathway is an unlikely therapeutic target for mtSOD1-induced ALS.

Results

PERK haploinsufficiency does not affect disease in *SOD1(G93A)* high-copy transgenic mice

We used a genetic approach to clarify the importance of the PERK pathway in mtSOD1-induced familial ALS. To this end, we crossed *G93A*-HC mice onto a *PERK*$^{+/-}$ background. PERK$^{+/-}$ mice have no clinical phenotype and display decreased phosphorylation of eIF2α with ER stress (32). In contrast, *PERK*$^{-/-}$ mice are normal at birth, but subsequently develop a rapid and progressive decline in endocrine and exocrine pancreatic functions, such that they could not be used in these studies (32). Progeny were followed for general disease progression by assessing their weight loss, muscle fatigue (using an inverted grid-hanging test), and survival. Males and females were analyzed separately. We found that both male and female *G93A*-HC and *G93A*- HC/*PERK*$^{+/-}$ mice displayed a nearly identical disease course, manifested by similar weight at all time points examined (Fig. 1A, B) and by comparable motor performance (Fig. 1C, D). We also found that *PERK* haploinsufficiency had no significant effect on the survival of *G93A*-HC mice (median survival: 171 d in *G93A*-HC versus 166 d in *G93A*-HC/*PERK*$^{+/-}$)(Fig. 4A).

We next evaluated molecular changes in tibialis anterior muscles and lumbar spinal cords of *G93A*-HC and *G93A*-HC/*PERK*$^{+/-}$ mice at 15 weeks of age, corresponding to an early disease stage, when the animals typically display hind limb tremor with tail suspension (graded as a clinical score of ‘1’ refer to “Methods” section for scoring system). Neuromuscular junction (NMJ) denervation is the first morphological change observed in ALS patients and mouse models (33). Because muscle denervation is associated with

functional motor deficits, preservation of NMJs is commonly used as a criterion to determine a meaningful effect on target modulation. We stained tibialis anterior muscles with antibodies against synapsin I (SynI) to label nerve terminals and with α- bungarotoxin (α-BGT) to visualize acetylcholine receptors (AChRs) in muscle. Quantitation revealed fully innervated synaptic sites in WT and PERK$^{+/-}$ control mice, with nerve terminals perfectly apposed to AChRs in the postsynaptic membrane. In contrast, *G93A*-HC and *G93A*- HC/*PERK*$^{+/-}$ transgenics displayed significant tibialis anterior denervation, although the extent of denervation was statistically similar for both groups of mice (Fig. 1E). For motor neuron analysis, we identified motor neurons in the ventral horn of lumbar spinal cord using immunofluorescent labeling of choline acetyltransferase (ChAT). The extent of neurodegeneration was statistically similar in *G93A*-HC and *G93A*-HC/*PERK*$^{+/-}$ mice (~30–40% motor neuron loss compared to age-matched controls) (Fig. 1F, G). Overall, these data demonstrate that in contrast to a previously published report using *G85R* mice (25), *PERK* haploinsufficiency in *G93A*-HC mice affects neither their disease course, nor histopathology.

GADD34 deficiency does not ameliorate disease in *SOD1(G93A)* high-copy transgenic mice

GADD34 is a stress-inducible regulatory subunit of a holophosphatase complex that dephosphorylates p-eIF2α and plays a role in translational recovery (34). It has been shown that inhibition of GADD34 enhances the UPR by prolonging the phosphorylation of eIF2α (35–37). To access the impact of GADD34 deficiency on familial ALS, we bred *GADD34*$^{\Delta C/\Delta C}$ mice, which express a mutation encoding a truncated GADD34 protein that lacks eIF2α phosphatase activity (36), with *G93A*-HC mice. The histopathology and disease progression of the offspring were then evaluated.

Previous genetic studies showed that *G85R* mice with diminished GADD34 activity (*G85R/GADD34*$^{+/\Delta C}$) display a delay in the onset of disease and a markedly prolonged survival (26). On the contrary, our data revealed no protection against weight loss (Fig. 2A, B) or progressive motor deficits (Fig. 2C, D) in *G93A*-HC/*GADD34*$^{\Delta C/\Delta C}$ mice compared to their *G93A*-HC littermates. Both male and female *G93A*-HC/*GADD34*$^{\Delta C/\Delta C}$ mice demonstrated significantly reduced motor performance on the inverted grid-hanging test compared to their age- and sex-matched *G93A*-HC littermates, although motor deficits were more pronounced in females versus males (Fig. 2C, D). Importantly, no significant change in survival was observed in *G93A*-HC/*GADD34*$^{\Delta C/\Delta C}$ mice compared to *G93A*-HC mice (median survival: 166 d versus 171 d) (Fig. 4B).

At the histopathological level, tibialis anterior muscles and lumbar spinal cords of *G93A*-HC/*GADD34*$^{\Delta C/\Delta C}$ and *G93A*-HC mice at an early diseases stage (15 weeks of age) displayed statistically similar extent of NMJ denervation (Fig. 2E) and motor neuron degeneration (Fig. 2F, G). Therefore, the loss of GADD34 activity did not exert a protective effect either at the level of the synapse (NMJ innervation), or the spinal cord (motor neuron numbers).

CHOP deficiency does not ameliorate disease in *SOD1(G93A)* high-copy transgenic mice

CHOP is a transcription factor downstream of the PERK-eIF2α pathway. CHOP activation has been shown to play an essential role in ER stress-induced apoptosis (21, 38, 39), although recent studies suggest that CHOP expression can be either adaptive or maladaptive, depending on cell type and disease context (40, 41). We investigated the role of CHOP in familial ALS using *CHOP*$^{-/-}$ mice, which are phenotypically normal, but display an attenuated response to ER stress (39). These mice were crossed with *G93A*-HC mice to obtain *G93A*-HC/*CHOP*$^{-/-}$ mice. Although we found that *G93A*-HC/*CHOP*$^{-/-}$ mice exhibited modestly accelerated weight loss compared to their age- and sex-matched *G93A*-HC littermates (Fig. 3A, B), these effects were not statistically significant. Nevertheless, the *G93A*-HC/*CHOP*$^{-/-}$ mice did display significantly reduced motor performance (on the inverted grid-hanging test) compared to their *G93A*-HC littermates (Fig. 3C, D). Interestingly, these motor deficiencies were more severe in males versus females. At the same time, the loss of CHOP did not affect survival in the transgenic mice (median survival: 171 d in *G93A*-HC versus 163 d in *G93A*-HC/*CHOP*$^{-/-}$) (Fig. 4C).

In parallel experiments, we examined tibialis anterior muscles and lumbar spinal cords collected from 15-week-old transgenic mice by immunohistochemistry. *G93A*-HC/*CHOP*$^{-/-}$ and G93A-HC mice had a statistically similar extent of NMJ denervation (Fig. 3E), as well as motor neuron degeneration (Fig. 3F, G). All together, these data indicate that the loss of CHOP is not protective against disease in *G93A*-HC mice.

The level of SOD1(G93A) expression does not determine the response to genetic modulation of the PERK pathway

In contrast to prior genetic studies conducted in *G85R* mice, we did not observe modulation of disease in *G93A*-HC mice by genetic ablation of key molecules in the PERK pathway. A possible explanation could involve the extent of the toxic effect of the over-expressed human *mtSOD1* gene. *G93A*-HC mice are characterized by extreme *mtSOD1* overexpression (42). As a result, *G93A*-HC mice display an aggressive disease phenotype, with an early disease onset and a shorter life span, compared to other mtSOD1 strains (Table 1). In contrast, *G85R* mice used in this study express *mtSOD1* at levels comparable to endogenous *SOD1* expression and develop a late-onset form of disease (at ~9.5 months of age, defined by the onset of weight loss) (43). However, once initiated, the disease proceeds very rapidly and mice are completely paralyzed within 2 to 4 weeks after initial symptoms. Considering these differences in the disease course of *G85R* and *G93A*-HC mice, we next examined a variant of the *G93A* strain that expresses more modest levels of the human transgene, and, therefore, undergoes a prolonged disease compared to *G93A*-HC mice (Table 1) (44). Importantly, the average survival time of these low-copy *G93A* mice (*G93A*-LC) is similar to that in *G85R* mice (~10 months of age for *G93A*-LC versus ~11 months of age for *G85R*), thus enabling a more direct comparison between these two strains.

We crossed *G93A*-LC mice with either *PERK*$^{+/-}$ or *GADD34*$^{\Delta C/\Delta C}$ mutant mice, and then followed the disease progression and survival in their progeny. We found that the *PERK*$^{+/-}$ mutation had no significant effect on weight in the *G93A*-LC mice, either in males or females (Fig. 5A, B). Additionally, no significant change was observed in median survival of

G93A- LC/*PERK*$^{+/-}$ mice compared to their *G93A*-LC littermates (286 d versus 288 d) (Fig. 5C). The analysis of *G93A*-LC/*GADD34*$^{\Delta C/\Delta C}$ animals revealed no protection against weight loss (Fig. 5D, E). The *G93A*-LC/*GADD34*$^{\Delta C/\Delta C}$ males displayed modestly reduced weights throughout the disease course compared to their male *G93A*-LC littermates (Fig. 5D)

however, these results were not statistically significant. Moreover, *G93A*-LC and *G93A*- LC/*GADD34*$^{\Delta C/\Delta C}$ mice had similar median survival times (295.5 d versus 296 d) (Fig. 5F). In agreement with our weight and survival studies, histological analysis of tibialis anterior muscles and lumbar spinal cords of early-symptomatic (8 months of age) *G93A*-LC and *G93A*- LC/*GADD34*$^{\Delta C/\Delta C}$ mice revealed a comparable extent of NMJ denervation (Fig. 5G) and motor neuron degeneration (Fig. 5H, I). These data suggest that the level of the *mtSOD1* transgene expression, and the associated protein toxicity, do not determine the response of mice carrying *G93A* mutation to genetic alterations in the PERK pathway.

Transgenic mice carrying different *SOD1* mutations respond similarly to genetic ablations of *PERK* and *GADD34*

One of the hypotheses regarding the molecular mechanisms of ALS is based on mutation-driven SOD1 misfolding and subsequent deposition of its cytotoxic aggregates. More than 100 different mutations have been found in the *SOD1* gene throughout all coding regions (45). It is generally thought that the different mtSOD1 proteins cause ALS by a similar mechanism, although it remains unclear how mutations in distinct *SOD1* regions can lead to similar disease manifestations. We considered the possibility that if the level of *mtSOD1* expression has little effect, then perhaps a specific mutation might determine the response of a *mtSOD1* mouse strain to genetic alterations in the PERK pathway.

To account for this possibility and further explore the discordant results in *G85R* and *G93A* mice, we investigated two additional well-characterized mtSOD1 mouse models: *G37R* mice, lines 42 and 29 (46). The *G37R*-42 mouse line is most similar to the *G93A*-HC line in respect to disease onset and survival (Table 1). The other *G37R* mouse line (*G37R*-29) has dramatically prolonged disease onset (~10 months of age) and survival (~17 months of age) (Table 1). As before, we crossed *G37R*-42 and *G37R*-29 mice with either *PERK*$^{+/-}$ or *GADD34*$^{\Delta C/\Delta C}$ mutants, and followed disease progression in their progeny. We discovered that neither *PERK* haploinsufficiency nor homozygous *GADD34* deficiency significantly affected weight gain/loss in *G37R*-42 mice (male or female) throughout the disease course (Fig. 6A, B, D, E). Genetic ablations of *PERK* and *GADD34* also had no significant effect on median survival of *G37R*-42 mice (192−195.5 d in *G37R*-42 versus 196 d in *G37R*-42/*PERK*$^{+/-}$ versus 185 d in *G37R*- 42/*GADD34*$^{\Delta C/\Delta C}$) (Fig. 6C, F). In parallel experiments, we followed the disease course of *G37R*-29/*PERK*$^{+/-}$ and *G37R*-29/*GADD34*$^{+/\Delta C}$ mice, as well as their control *G37R*-29 littermates. Due to the exceedingly long life span of *G37R*-29 mice, we chose to follow them until 14.5 months of age (early-symptomatic disease), when the mice display a clinical score of ‘1’. We found that *PERK* haploinsufficiency had no effect on weight trend in *G37R*-29/*PERK*$^{+/-}$ mice (Fig. 7A). At the same time, *G37R*-29/*GADD34*$^{+/\Delta C}$ mice exhibited modestly reduced weight gain early in the disease course compared to *G37R*-29 mice, although not statistically significant (Fig. 7B). Nonetheless,

these weight data suggest that *GADD34* haploinsufficiency is not protective against disease. To confirm these findings at the histological level, we analyzed tibialis anterior muscles and lumbar spinal cords collected from 14.5-month-old *G37R*- 29/*PERK*$^{+/-}$ and *G37R*-29/*GADD34*$^{+/\Delta C}$ mice and their respective age-matched *G37R*-29 littermates. Although both complete NMJ denervation and motor neuron loss were observed in these two double-transgenic groups, the extent of the pathology was not significantly different from that in *G37R*-29 mice (Fig. 7C–H).

The original findings that demonstrated the potential involvement of the UPR in mtSOD1-induced ALS used the *G85R* mice (47). As none of the four mouse models we used in our study demonstrated a significant effect on disease after genetic inhibition or enhancement of the UPR-PERK pathway, we decided to investigate the effects of genetic *PERK* and *GADD34* deficiencies in the *G85R* mouse model. Because the original *G85R* mouse line (47) was no longer available, we used another *G85R* mouse line (43). We bred these mice with *PERK*$^{+/-}$ and *GADD34*$^{\Delta C/\Delta C}$ mutants, and analyzed the resulting *G85R*/*PERK*$^{+/-}$ and *G85R*/*GADD34*$^{\Delta C/\Delta C}$ double-mutant offspring. Based on our experimental data, the *G85R* mouse line is distinct from other mtSOD1 lines (Table 1) in that early clinical symptoms (equivalent to a score of ‘1’ or ‘2’, denoting the severity of limb tremors) are not observed. As the first clinical symptom is limb paralysis (equivalent to a score of ‘3’), we selected time points (9.5–10 months of age) that were prior to the typical onset of limb paralysis and corresponded to the average disease onset/early disease to end our observations and collect histological samples. In contrast to a prior study (25), we did not observe an earlier disease onset in *G85R*/*PERK*$^{+/-}$ mice. Although it was previously reported that mean disease onset (defined as peak weight before a decline) of *G85R*/*PERK*$^{+/-}$ mice was at ~8.5 months of age (25), in our study *G85R* and *G85R*/*PERK*$^{+/-}$ animals displayed a similar trend of weight gain until 9.5 months of age, corresponding to disease onset in *G85R* mice and the last time point examined (Fig. 8A). We also analyzed tibialis anterior muscles and lumbar spinal cords collected from 9.5-month-old animals and did not observe accelerated neuropathological changes in *G85R*/*PERK*$^{+/-}$ mice compared to *G85R* mice (Fig. 8C–E). Similarly, comparisons of the weight gain trends in *G85R*/*GADD34*$^{\Delta C/\Delta C}$ and *G85R* mice revealed no statistically significant differences between these two groups of mice until 10 months of age, the last time point examined (Fig. 8B). The immunohistochemical analysis of NMJ innervation in tibialis anterior muscles of *G85R*/*GADD34*$^{\Delta C/\Delta C}$ and G85R mice at 10 months of age demonstrated a comparable extent of modest endplate denervation in both groups of mice (Fig. 8F), suggesting that in contrast to a prior study (26), *GADD34* deficiency is not protective against disease. As expected from precipitous disease course in *G85R* mice, where significant motor neuron loss occurs shortly before end-stage disease (~11 months of age), motor neuron numbers in lumbar spinal cords of 10-month-old *G85R*/*GADD34*$^{\Delta C/\Delta C}$ and *G85R* mice were found to be normal (Fig. 8G, H). Cumulatively, these data demonstrate that all five mtSOD1 mouse strains studied show a similar response, or lack thereof, to genetic alterations in the PERK pathway.

Biochemical analyses of the PERK pathway in spinal cords of early-symptomatic and end-stage mutant SOD1 mice

It was previously suggested that alterations to ER proteostasis play a critical role in ALS progression and represent one of the earliest pathological signatures of the disease (48). We therefore investigated molecular changes in lumbar spinal cords of early-symptomatic and paralyzed (end-stage) mtSOD1 mice (Table 1) by real-time qPCR and by western blot. We found no change in *GADD34* and *CHOP* mRNA expression levels at an early disease stage in all five mtSOD1 mouse strains used in the study (Fig. 9A, Fig. S1A). Consistent with mRNA expression data, we also did not observe any changes in GADD34 and CHOP protein levels. Additionally, there was no evidence of increased phosphorylation of eIF2α at this early disease time point in all five mtSOD1 mouse strains examined (Fig. 9C, D and Fig. S1B, C). Interestingly, there was an increase in protein levels of the downstream UPR transcription factor ATF4 at an early disease stage (Fig. 9C, D and Fig. S1B, C), despite the apparent absence of PERK pathway activation. Together, our results indicate that PERK pathway activation is not detected early in disease (when mice have started to display clinical symptoms), at least not at the level of total RNA and protein analyses in lumbar spinal cord lysates.

In mice with end-stage disease, we observed an increase in *GADD34* mRNA levels in the *G85R* mice, and in *CHOP* mRNA levels in the *G37R*-42 mice (Fig. 9B). However, there was no correlation between message and protein levels (the latter were reduced or unchanged) (Fig. 9E). Also in these mice, the enhanced phosphorylation of eIF2α was surprisingly not accompanied by an increase in GADD34 and CHOP protein levels. On the contrary, GADD34 protein levels were significantly reduced, whereas CHOP protein levels remained unchanged, relative to those in similarly aged wild-type control littermates. These results were consistent across all four mtSOD1 mouse strains analyzed (Fig. 9C, E). Additionally, we found that whereas *ATF4* mRNA levels remained unaffected, the ATF4 protein levels were significantly upregulated in end-stage disease (Fig. 9B, C, E). These data demonstrate that increased phosphorylation of eIF2α in lumbar spinal cords of all end-stage mtSOD1 mouse strains examined does not result in a full UPR response.

Discussion

ALS is associated with the accumulation of abnormal intracellular protein aggregates, which can disrupt the balance between protein generation and degradation that is crucial for protein homeostasis. These alterations can trigger ER stress and ultimately contribute to neurodegeneration. Cells counteract ER stress by activating the UPR, which aims to restore proteostasis within the secretory pathway in part through regulation of genes involved in protein folding, quality control, degradation and translational repression pathways (49). PERK is the most rapidly activated UPR pathway in response to the accumulation of misfolded proteins, leading to eIF2α phosphorylation and subsequent attenuation of protein synthesis (50). The PERK/eIF2α phosphorylation axis recently emerged as a potential therapeutic target for ALS (51, 52). Therefore, we sought to conduct a comprehensive analysis of the effects of genetic PERK pathway modulation on ALS using several well-characterized mtSOD1 transgenic mouse models. We demonstrate that, in contrast to

previous reports (25, 26), neither *PERK* haploinsufficiency nor *GADD34* deficiency significantly affect survival in all mtSOD1 mouse models examined. Moreover, we show that genetic ablation of the pro-apoptotic *CHOP* transcription factor has no effect on survival in *G93A*-HC mice. Overall, our data show an absence of disease modulation by genetic alteration of the key molecules in the PERK pathway.

It was previously reported that *G85R/PERK*$^{+/-}$ mice display an accelerated disease course and pathology (25). In contrast, we discovered that *PERK* haploinsufficiency had no effect on disease in all five mtSOD1 mouse models studied, including the *G85R* mice. We further discovered that these divergent findings were not likely due to the level of the *mtSOD1* transgene expression, as the *PERK*$^{+/-}$ mutation had no effect on disease progression and survival of both *G93A*-HC and *G93A*-LC mouse lines. Moreover, we found that transgenic mice carrying different SOD1 mutations displayed similarly unchanged disease and pathology in response to *PERK* haploinsufficiency. Taken together, our genetic data suggest that PERK signaling does not likely play a crucial role in mtSOD1-induced ALS.

With regards to *G85R* mice, our disparate results from what has been published (25) might reflect the use of distinct *G85R* transgenic lines, which were generated by different laboratories. Specifically, *G85R* transgenic mice used in the original UPR genetic studies (25, 26), but no longer available, were generated with a construct containing *loxP* sites engineered to flank the *G85R* mutant human *SOD1* gene (47). These mice reportedly over-express the human SOD1 protein at levels approximately 50% higher than the endogenous mouse SOD1 protein, which may augment the development of ER stress in these animals. In contrast, we used transgenic mice that carry a *G85R* mutant human *SOD1* transgene lacking the *loxP* sequences (43). These mice express the human SOD1 protein at levels comparable with the endogenous mouse SOD1 protein. Therefore, the lack of an effect on the mtSOD1 phenotype by the genetic manipulation of the UPR in the current study might reflect our use of a *G85R* mouse line that expresses more physiologically relevant levels of the mtSOD1 protein. Notably, similar discrepancies between these two *G85R* lines have been previously recognized (47). Our results thus caution against drawing conclusions regarding mechanistic contributors to ALS pathogenesis from a single mutant SOD1 mouse line. Additionally, it is important to mention that mutant SOD1 mouse lines display significant variability with regards to disease onset and progression (Table 1). This variability is currently unexplained, but may be an important factor that should be taken into consideration as far as translational efforts are concerned.

In agreement with our genetic studies, we did not observe PERK pathway activation at the molecular level in lumbar spinal cords of early-symptomatic mtSOD1 mice, which by that time already exhibited substantial neuropathological changes. These included significant motor neuron loss in the ventral horn of lumbar spinal cords and NMJ denervation in tibialis anterior muscles. The protein levels of p-eIF2α, as well as mRNA and protein levels of GADD34 and CHOP, were consistently unchanged in all mtSOD1 mouse strains analyzed, suggesting that PERK signaling is not involved in early disease. There is a possibility, however, that the UPR mRNA and protein expression levels were very low and thus below the sensitivity of detection using our real-time qPCR and western blot assays (in whole lumbar spinal cord lysates). It was previously suggested that adaptation to ER stress in cells

chronically exposed to protein folding insults, such as those implicated in familial forms of neurodegeneration, is an intrinsic consequence of low-level activation of the UPR (53). This is in contrast to robust UPR activation in cells by acute severe stress, such as pharmacological perturbation of ER function. Along the same lines, prior evidence of ER stress activation specifically in motor neurons of mtSOD1 mice with early disease (9, 11) suggests that our analyses of whole lysates may not have detected changes that occurred exclusively in motor neurons.

Under ER stress, persistent activation of the PERK/eIF2α pathway, and the resulting global suppression of protein synthesis, play a major role in determining the cell's fate. GADD34 (also known as PPP1R15A) is a stress-inducible regulatory subunit of the PP1/GADD34 holophosphatase complex that quickly dephosphorylates p-eIF2α to counteract PERK signaling and restore general protein synthesis. Recently, pharmacological targeting of GADD34-mediated p-eIF2α dephosphorylation has emerged as a promising strategy for modifying the course of protein misfolding diseases, including ALS (51, 52, 54). To this end, several small molecule inhibitors (salubrinal, guanabenz, and Sephin1) have been used to disrupt the PP1/GADD34 holophosphatase complex in order to enhance eIF2α phosphorylation and downstream signaling. Salubrinal attenuated disease manifestations and prolonged survival in the *G93A*-HC mouse model (9), while guanabenz ameliorated disease in two separate studies using *G93A*-HC mice (28, 29). Nevertheless, another group reported adverse effects of guanabenz in *G93A*-HC mice. In these studies, guanabenz treatment significantly accelerated disease onset and shortened lifespan in male mice (30). Most recently, Sephin1 prevented motor deficits and motor neuron loss in *G93A*-HC mice (27).

The divergent findings using small-molecule GADD34 inhibitors highlight some of the challenges of pharmacological modulation of the ER stress response in mouse models of ALS. These include issues of bioavailability, potency, specificity, or off-target effects that can be associated with using pharmacological compounds. Moreover, given that pharmacological studies were all conducted in the *G93A*-HC mouse model, we were interested in analyzing the effects of *GADD34* deficiency in these transgenic mice by using a genetic approach. We discovered that, in direct contrast to a genetic study using *G85R* mice (26), as well as the pharmacological studies, *GADD34* deficiency did not ameliorate disease in *G93A*-HC mice, and did not affect their survival. Importantly, GADD34 deficiency similarly did not alleviate disease in all other mtSOD1 mouse models studied, including the *G85R* model. The inconsistency of our genetic study and the pharmacological studies might suggest that the consequences of genetic *GADD34* ablation during development are different from transient pharmacological inhibition of GADD34 in the adult. It is known that genetic knockout or knockdown approaches can produce phenotypes distinct from those seen with drug perturbation (55). A limitation of our *G85R*/*GADD34*$^{\Delta C/\Delta C}$ study is that we followed *G85R*/*GADD34*$^{\Delta C/\Delta C}$ mice and their *G85R* littermates only to 10 months of age (corresponding to early disease in control *G85R* mice), at which time lumbar spinal cord and tibialis anterior muscle tissues were collected for immunohistochemical analysis. At this time point, we did not detect significant differences in the extent of NMJ denervation in *G85R*/GADD34$^{\Delta C/\Delta C}$ mutant mice compared to their *G85R* littermates. Nevertheless, since none of our survival studies, which were carried out in *G93A*-HC, *G93A*-LC, and *G37R*-42 mouse strains, revealed a positive protective effect of

the GADD34 mutation, it is possible that *G85R* mice are the only ones that show disease modulation by genetic *GADD34* haploinsufficiency. In this case, it might be an indication that the outcomes are model-specific and possibly uninformative for human disease.

CHOP is a key transcription factor in the PERK pathway and is known to play an important role in ER stress-mediated cell death (21, 38, 39). There is also evidence suggesting that CHOP expression can be adaptive or maladaptive, depending on cell type and disease context. For instance, genetic *CHOP* ablation was shown to be detrimental to hippocampal neurons after seizures (40, 56), but neuroprotective in EAE/optic neuritis (57), Parkinson's disease (58), and moderate spinal cord injury (59). Increased CHOP expression has been detected in spinal cords of sporadic ALS patients and familial ALS mouse models (5, 31). At the same time, the exact role of CHOP in ALS is not clear. Considering that in the ER stress response CHOP is a critical player that can decide cellular fate, it is important to determine whether CHOP could be a viable target for therapeutic intervention. We hypothesized that genetic *CHOP* deletion will be protective in *G93A*-HC mice. On the contrary, we discovered that *CHOP* deficiency did not ameliorate disease in these mice. There was also no significant difference in the survival between *G93A*-HC/*CHOP*$^{-/-}$ and littermate *G93A*-HC mice, indicating that global *CHOP* deletion ultimately does not affect disease outcome. Therefore, the present study demonstrates that the PERK-CHOP signaling axis is unlikely to be significantly involved in mtSOD1-induced ALS.

Conclusions

In summary, we have investigated the role of the UPR-PERK pathway in mtSOD1-induced ALS using several transgenic mouse models. Our gene expression data suggest that PERK pathway might not be a prominent player in mtSOD1-induced disease. These results are in agreement with our genetic studies, where neither inhibition of the ER stress response (via ablation of *PERK*), nor ER stress response enhancement (via ablation of *GADD34*), had a significant effect on the survival of mtSOD1 mice. We also showed that genetic *CHOP* ablation is not protective against the disease. Therefore, targeting the PERK arm of the UPR is not likely to be an effective strategy for ALS therapy.

Materials and Methods

Animals

Mice overexpressing human *SOD1* (*hSOD1*) were purchased from Jackson Laboratory (Bar Harbor, ME). The following mutant *SOD1* strains were used: B6.Cg-Tg(SOD1-G93A)1Gur/J (stock #004435), B6.Cg-Tg(SOD1-G93A)^{dl}1Gur/J (stock #002299), B6.Cg-Tg(SOD1- G37R)42Dpr/J (stock #008342), B6.Cg-Tg(SOD1-G37R)29Dpr/J (stock #008229), and B6.Cg- Tg(SOD1-G85R)148Dwc/J (stock #008248). These mutant *SOD1* mice have been previously described (42–44, 46) and were maintained in-house as hemizygous transgenics. *GADD34*$^{\Delta C/\Delta C}$ and *PERK*$^{+/-}$ mice were kindly provided by Dr. David Ron (University of Cambridge, Cambridge, UK), and *CHOP*$^{-/-}$ mice were purchased from Jackson Laboratory (stock #005530). These mice have been previously described (32, 36, 39) and were bred in-house. All mice were on the C57BL/6 background. Both males and females were used.

All mice used in this study were housed under pathogen-free conditions at controlled temperatures and relative humidity with a 12/12-hour light/dark cycle and free access to pelleted food and water. All animal experiments were conducted in compliance with The University of Chicago's Animal Care and Use Committee guidelines.

Genotyping

Mouse genomic DNA was isolated from tail biopsies and amplified using REDExtract-N-Amp™ Tissue PCR Kit (catalog# XNAT, Sigma-Aldrich) as per manufacturer's instructions. Genotyping PCRs were performed using the following primer sequences: human SOD1 sense (5'- CATCAGCCCTAATCCATCTGA-3') and human SOD1 anti-sense (5'-CGCGACTAACAATCAAAGTGA-3') primers were used in combination with positive control mouse interleukin-2 (IL-2) sense (5'-CTAGGCCACAGAATTGAAAGATCT-3') and mouse IL-2 anti-sense (5'-GTAGGTGGAAATTCTAGCATCATCC-3') primers. IL-2 PCR product was visualized at 324 bp and human SOD1, if present, at 236 bp. PERK sense primer (5'- CGGAGACAGTACAAGCGCAGATGA-3') was used with either wild-type (wt) PERK anti-sense primer (5'- AAGGACCCTATCCTCCTGCTGCAC-3') or mutant (mt) PERK anti-sense primer (5'- GCTACCGGTGGATGTGGAATGTG-3') in separate reactions. Expected bands were 232 bp (wt), 302 bp (mt). GADD34 sense primer (5'-CCAGGAGAGAAGACCAAGGGACGTG-3') was used in combination with wt GADD34 anti-sense primer (5'- CGAGATTGCAAGAGAGTGAACACAGC) and mt GADD34 anti-sense primer (5'- AAGCCTTCGCCATCTGCTTATCCAG-3') in a single reaction. Expected bands were 468 bp (wt), 550 bp (mt). CHOP sense primer (5'-ATGCCCTTACCTATCGTG-3') was used with wt CHOP anti-sense primer (5'-GCAGGGTCAAGAGTAGTG-3') and mt CHOP anti-sense primer (5'-AACGCCAGGGTTTTCCCAGTCA-3') in a single reaction. Expected bands were 544 bp (wt), 320 bp (mt).

hSOD1 copy number assessment

It was previously reported that the phenotype of high-copy G93A mice is dependent on the number of transgene copies in their genome (60). Because the mutant *G93A* transgene can sometime undergo copy number loss due to intra-locus recombination events during meiosis, it is imperative to monitor the transgene number in the breeding colony (61). To this end, we determined the *SOD1(G93A)* copy number using a real-time qPCR assay in all breeders and their progeny. Genomic DNA was extracted from tails with the use of an Extract-N-Amp tissue PCR kit (catalog# XNAT2R, Sigma-Aldrich). The following primers and probes (Integrated DNA Technologies Inc.) were used, as suggested by Jackson Laboratory: human SOD1 sense primer (5'-GGGAAGCTGTTGTCCCAAG-3') human SOD1 anti-sense primer (5'-CAAGGGGAGGTAAAAGAGAGC-3') human SOD1 FAM probe (5'-CTGCATCTGGTTCTTGCAAAACACCA-3') mouse apolipoprotein-B (internal control) sense primer (5'-CACGTGGGCTCCAGCATT-3') mouse apolipoprotein-B anti-sense primer (5'-TCACCAGTCATTTCTGCCTTTG-3') mouse apolipoprotein-B Cy5 probe (5'-CCAATGGTCGGGCACTGCTCAA-3'). Extract-N-AMP PCR ReadyMix reagent (catalog #E3004, Sigma-Aldrich) was used for real-time amplification of DNA. After heating at 94°C for 3 min, the DNA was amplified by 40 cycles of 94°C for 15 s and 60°C for 1 min on a Bio-Rad CFX96 Real-Time PCR detection system. The transgene zygosity was determined

by comparing ΔC(t) values of each SOD1-positive sample against standard high-copy controls, using an endogenous reference (apolipoprotein-B). We found that the copy number did not change over multiple generations and the course of experiments.

Clinical assessment and survival

Transgenic SOD1-positive mice and their littermate controls were followed for disease onset, progression, and survival as previously described in studies of familial ALS mouse models (61, 62). Weight was recorded twice a week for *SOD1*(*G93A*) high-copy mice and once a week for all other *mtSOD1* strains. Onset of the disease was defined as peak weight before a decline (as a measure of denervation muscle atrophy onset). End-stage disease was defined by the inability of a mouse to right itself within 20 s after being placed on its side. This artificial endpoint is used to determine 'survival' reliably and humanely. In addition to weight, the neurological score of limbs was assessed at least once a week on a scale from 0 to 4 (with 0= normal, 1= hind limb tremor with tail suspension, 2= tremor with locomotion, 3= limb paralysis, and 4= mouse paralyzed and cannot right itself within 20 s after being placed on its side). The neurological assessment was necessary to identify non-ALS deaths: if a mouse dies before attaining a score of '2', it is highly unlikely that the death is attributable to ALS. Additionally, to facilitate access to food and hydration, wet food pellets and gel diet were placed on the cage floor when the animals developed limb paralysis.

Behavioral test for high-copy *SOD1(G93A)* mice

Motor fatigue was assessed once a week, starting at 8 weeks of age, using an inverted grid-hanging test (63, 64). Individual mice were placed in the center of a wire grid, which was mounted ~80 cm above a padded surface. The grid was then gently inverted and maintained in an inverted position for 60 s. The length of time each mouse remained attached to the grid was recorded. Each mouse was tested three times with an interval of ~15 min. The average hanging time was calculated from two best attempts. Control mice routinely remained attached to the grid for the entire duration of the experiment. For mtSOD1-positive mice, the experiment was stopped once hanging time was less than 5 s, at approximately 19 to 21 weeks of age.

Histology

Mice were deeply anaesthetized with 2.5% avertin in dH_2O. Avertin stock solution was prepared by dissolving 2, 2, 2-Tribromoethanol (catalog #T48402, Sigma Aldrich) in 2-methyl-2-butanol (catalog #240486, Sigma Aldrich). Upon the loss of nociceptive reflexes, animals were perfused transcardially with 0.9% NaCl, followed by cold 4% PFA in PBS. Tibialis anterior muscles were immediately dissected out. Whole muscles were post-fixed in 4% PFA for 20 min and rinsed in PBS for 5 min, followed by cryopreservation through 3 successive 5 min incubations in 5, 10, and 15% sucrose in PBS. Tissue samples were then incubated overnight in 20% sucrose in PBS, embedded in Optimal Cutting Temperature compound (OCT) and frozen on dry ice. Spinal cords were carefully dissected out, post-fixed in 4% PFA for 4 h, washed in PBS, and cryopreserved in 30% sucrose until saturation. The lumbar segments of each spinal cord were embedded in OCT and frozen on dry ice. Samples were stored in −80°C until use.

Immunohistochemistry

Longitudinal tibialis anterior muscle sections were cut at 10 μm on a cryostat, collected onto microscope slides (catalog #1358W, Globe Scientific Inc), and frozen at −80°C until use. For immunostaining, sections were allowed to thaw at room temperature (RT), permeabilized in acetone at −20°C for 10 min and washed with PBS. Sections were then incubated for 1 h at RT in a blocking solution, consisting of PBS, 5% BSA, 1% normal donkey serum, and 0.2% Triton X-100. Primary antibody staining was performed overnight at 4°C in a humidifying chamber with antibodies diluted in the blocking solution. To analyze the NMJs in tibialis anterior muscles, presynaptic nerve terminals were detected with rabbit 1:500 synapsin I antibody (catalog #ab18814, Abcam), and postsynaptic endplates (AChRs) with 1:200 Alexa 594-conjugated α- bungarotoxin (α-BGT) (catalog #B13423, Life Technologies). Sections were then rinsed 3 times with PBS, and secondary donkey-anti-rabbit IgG Alexa 488 antibody (Life Technologies) was applied for 2 h at RT. For lumbar spinal cords, transverse sections were cut at 10 μm on a cryostat, collected onto microscope slides (catalog #1358W, Globe Scientific Inc), and frozen at −80°C until use. Immunostaining was performed using an antigen retrieval technique. Briefly, sections were washed in TBS (pH 7.5), and boiled in 10mM trisodium citrate buffer (pH 6.0) for 30 min at 90°C, followed by cooling at RT for 30 min. Sections were then incubated in 10 mM glycine (in TBS with 0.25% Triton X-100) for 1h at RT to quench autofluorescence from the PFA. After several washes in TBS, blocking solution was applied for 1 h at RT, followed by overnight incubation with goat 1:200 choline acetyltransferase antibody (ChAT) (catalog #AB144P, Millipore) to visualize motor neurons. Secondary donkey-anti-goat IgG Alexa 594 antibody (Invitrogen) was applied in the blocking solution for 2 h at RT. The fluorescent-stained muscle and spinal cord tissue sections were mounted in ProLong Gold antifade reagent with DAPI (catalog # P36931, Thermo Fisher Scientific) under a glass coverslip. Tissue sections were imaged with Marianas Yokogawa type spinning disk confocal microscope using 20x Plan- Neofluar/NA 0.5 dry objective.

For muscle innervation analysis, we examined 50–100 neuromuscular junctions (NMJs) in tibialis anterior of each mouse (n=3–4 animals per genotype). Each NMJ was designated as fully innervated, partially denervated, or fully denervated. At fully innervated NMJs, nerve terminal staining completely overlapped with α-BGT staining for postsynaptic AChRs, whereas fully denervated NMJs displayed α-BGT staining only. At partially innervated NMJs, just a portion of the AChR-rich postsynaptic endplate was labeled with nerve terminal staining. Muscle innervation data (full/partial/none) were expressed as a percentage of total NMJs counted per animal. For motor neuron analysis, we defined motor neurons as cells in the ventral horn of the spinal cord that were positive for ChAT. We analyzed 4 non-consecutive lumbar spinal cord sections per mouse (n=3–4 animals per genotype). All immunohistochemistry analyses were done using mice in an early-symptomatic disease stage, as described in Table 1.

Total protein and RNA isolation

For spinal cord collection, deeply anesthetized mice were perfused with ice-cold PBS. Fresh lumbar spinal cords were then obtained by ejection of the cord from the vertebrate column (65) using a 18 g 1/2” needle (BD Biosciences) attached to a 10-mL syringe filled with PBS.

Spinal cord tissues were rinsed in PBS, snap frozen in liquid nitrogen, and stored in −80°C until use.

For protein isolation, samples were homogenized in ice-cold RIPA lysis buffer (catalog #R0278, Sigma-Aldrich) supplemented with protease inhibitor cocktail (catalog #78430, Thermo Fisher Scientific), phosphatase inhibitor cocktail 2 (catalog #P2850, Sigma-Aldrich), phosphatase inhibitor cocktail 3 (catalog #P5726, Sigma-Aldrich), and 17.5 mM β-glycerophosphate (catalog #G9422, Sigma- Aldrich). After 30 min incubation on ice, protein lysates were clarified by centrifugation at 14,000 rpm for 20 min at 4°C, and stored at −80°C. Protein concentration was determined using a BCA Protein Assay Kit (catalog #23255, Thermo Fisher Scientific).

Total RNA was extracted from samples using Aurum Total RNA Fatty and Fibrous Tissue Kit (catalog #732–6870, Bio-Rad Laboratories). RNA concentration was measured with Nanodrop spectrophotometer, and RNA quality was confirmed on a model 2100 Bioanalyzer using Agilent RNA 6000 Nano Kit (catalog #5067–1511, Agilent Technologies) according to the manufacturer's instructions. Only samples with an RNA integrity number ≥ 8 were used.

Western blot

Protein samples (30 μg) were separated by SDS-PAGE using a 4–20% gradient gel, and transferred to a nitrocellulose membrane, pore size 0.2 μm (catalog #1620112, Bio-Rad). Nonspecific binding was blocked with 4% non-fat milk in TBST for 1 h at RT. Membranes were then incubated with primary antibodies in the blocking solution at 4°C overnight. The following primary antibodies were used: rabbit 1:500 p-eIF2α (catalog #AB32157, Abcam), rabbit 1:1000 eIF2α (catalog #9722S, Cell Signaling Technology), mouse 1:500 CHOP (catalog #MA1–250, Thermo Fisher Pierce), mouse 1:250 CHOP (catalog #sc-7351, Santa Cruz), mouse 1:250 ATF4 (catalog #sc-390063, Santa Cruz), rabbit 1:2000 GADD34 (catalog #sc-825, Santa Cruz), and mouse 1:2000 β-actin (catalog #A4700, Sigma- Aldrich). Proteins were stained with species-specific HRP-conjugated secondary antibodies (GE Healthcare) and visualized with Super Signal West Pico Chemiluminescent substrate (Thermo Fisher Scientific) on ChemiDoc™ Touch machine (Bio-Rad). Bands were quantified using Image Lab software (Bio-Rad). Data were normalized to β-actin and expressed as mean fold change in relation to the control group.

Quantitative real-time PCR

RNA was cleaned of genomic DNA, and reverse-transcribed, using iScript gDNA Clear cDNA Synthesis Kit (catalog #172–5035, Bio-Rad Laboratories) according to the manufacturer's instructions. Quantitative real-time PCR was run on a Bio-Rad CFX96 Real-Time PCR detection system using SYBR Green technology (catalog #1725271, Bio-Rad Laboratories). Relative gene expression was calculated using the ΔΔC(t) method after normalization to β-actin reference gene. Primers used (Integrated DNA Technologies Inc) are listed below:

Real-time qPCR primer sequences (Forward: Fwd Reverse: Rev).

CHOP

Fwd: 5’-CTGCCTTTCACCTTGGAGACG-3’

Rev: 5’-CTTTGGGATGTGCGTGTGACC-3’

GADD34 Exon 2

Fwd: 5’-CCCTCCAACTCTCCTTCTTCAG-3’

Rev: 5’-CAGCCTCAGCATTCCGACAA-3’

GADD34 Exons 2–3

Fwd: 5’-CCCGAGATTCCTCTAAAAGCTC-3’

Rev: 5’-CCAGACAGCAAGGAAATGG-3’

PERK

Fwd: 5’-TCTTGGTTGGGTCTGATGAAT-3’

Rev: 5’-GATGTTCTTGCTGTAGTGGGGG-3’

ATF4

Fwd: 5’-TGGATGATGGCTTGGCCAGTG-3’

Rev: 5’-GAGCTCATCTGGCATGGTTTC-3’

β-ACTIN

Fwd: 5’-GTGACGTTGACATCCGTAAAGA-3’

Rev: 5’-GCCGGACTCATCGTACTCC-3’

Statistical Analyses

Data are presented as mean ± SEM. Multiple comparisons were made using one-way ANOVA, or two-way repeated measures (RM) ANOVA, with Tukey’s post hoc test. Comparisons of two data points were made using a two-sided unpaired *t* test, with Holm-Sidak correction for multiple comparisons, where indicated. Comparisons of survival curves were made using log-rank (Mantel-Cox) test. A *P* value of <0.05 was considered significant. All statistical analyses were done using GraphPad Prism software.

Supplementary Material

Refer to Web version on PubMed Central for supplementary material.

Acknowledgements

We are grateful to Sharon Way for critical reading of the manuscript. We also thank Ani Solanki for technical assistance with the mice.

Funding

This work was supported by grants to BP from NIH/NINDS (R01 NS034939), Target ALS, and the Dr. Miriam and Sheldon G. Adelson Medical Research Foundation, and to YD from NIH/NINDS (F32NS089290).

Abbreviations

ALS	Amyotrophic lateral sclerosis
mtSOD1	Mutant superoxide dismutase 1
ER	Endoplasmic reticulum
UPR	Unfolded protein response
PERK	Protein kinase RNA-activated (PKR)-like ER kinase
GADD34	Growth arrest and DNA damage-inducible 34
CHOP	C/EBP homologous protein
ATF4	Activating transcription factor 4
eIF2α	Eukaryotic translation initiation factor 2α
NMJ	Neuromuscular junction
SynI	Synapsin I
AChR	Acetylcholine receptor
α-BGT	α-Bungarotoxin
ChAT	Choline acetyltransferase
WT	Wild-type
qPCR	Quantitative polymerase chain reaction
RT	Room temperature
PFA	Paraformaldehyde
BSA	Bovine serum albumin
PBS	Phosphate-buffered saline
TBS	Tris-buffered saline
OCT	Optimal cutting temperature compound
RM-ANOVA	Repeated-measures analysis of variance

References

1. Cleveland DW & Rothstein JD (2001) From Charcot to Lou Gehrig: deciphering selective motor neuron death in ALS. Nature reviews. Neuroscience 2(11):806–819. [PubMed: 11715057]
2. Gordon PH (2013) Amyotrophic Lateral Sclerosis: An update for 2013 Clinical Features, Pathophysiology, Management and Therapeutic Trials. Aging and disease 4(5):295–310. [PubMed: 24124634]
3. Rezania K & Roos RP (2013) Spinal cord: motor neuron diseases. Neurologic clinics 31(1):219–239. [PubMed: 23186902]
4. Rothstein JD (2009) Current hypotheses for the underlying biology of amyotrophic lateral sclerosis. Annals of neurology 65 Suppl 1:S3–9. [PubMed: 19191304]
5. Ito Y, et al. (2009) Involvement of CHOP, an ER-stress apoptotic mediator, in both human sporadic ALS and ALS model mice. Neurobiology of disease 36(3):470–476. [PubMed: 19733664]
6. Kikuchi H, et al. (2006) Spinal cord endoplasmic reticulum stress associated with a microsomal accumulation of mutant superoxide dismutase-1 in an ALS model. Proceedings of the National Academy of Sciences of the United States of America 103(15):6025–6030. [PubMed: 16595634]
7. Nagata T, et al. (2007) Increased ER stress during motor neuron degeneration in a transgenic mouse model of amyotrophic lateral sclerosis. Neurological research 29(8):767–771. [PubMed: 17672929]
8. Sasaki S (2010) Endoplasmic reticulum stress in motor neurons of the spinal cord in sporadic amyotrophic lateral sclerosis. Journal of neuropathology and experimental neurology 69(4):346–355. [PubMed: 20448480]
9. Saxena S, Cabuy E, & Caroni P (2009) A role for motoneuron subtype-selective ER stress in disease manifestations of FALS mice. Nature neuroscience 12(5):627–636. [PubMed: 19330001]
10. Walker AK & Atkin JD (2011) Stress signaling from the endoplasmic reticulum: A central player in the pathogenesis of amyotrophic lateral sclerosis. IUBMB life 63(9):754–763. [PubMed: 21834058]
11. Sun S, et al. (2015) Translational profiling identifies a cascade of damage initiated in motor neurons and spreading to glia in mutant SOD1-mediated ALS. Proceedings of the National Academy of Sciences of the United States of America 112(50):E6993–7002. [PubMed: 26621731]
12. Boillee S, Vande Velde C, & Cleveland DW (2006) ALS: a disease of motor neurons and their nonneuronal neighbors. Neuron 52(1):39–59. [PubMed: 17015226]
13. Bruijn LI, et al. (1998) Aggregation and motor neuron toxicity of an ALS-linked SOD1 mutant independent from wild-type SOD1. Science 281(5384):1851–1854. [PubMed: 9743498]
14. Ilieva H, Polymenidou M, & Cleveland DW (2009) Non-cell autonomous toxicity in neurodegenerative disorders: ALS and beyond. The Journal of cell biology 187(6):761–772. [PubMed: 19951898]
15. Nishitoh H, et al. (2008) ALS-linked mutant SOD1 induces ER stress- and ASK1- dependent motor neuron death by targeting Derlin-1. Genes & development 22(11):1451–1464. [PubMed: 18519638]
16. Ye Y, Shibata Y, Yun C, Ron D, & Rapoport TA (2004) A membrane protein complex mediates retro-translocation from the ER lumen into the cytosol. Nature 429(6994):841–847. [PubMed: 15215856]
17. Hetz C (2012) The unfolded protein response: controlling cell fate decisions under ER stress and beyond. Nature reviews. Molecular cell biology 13(2):89–102. [PubMed: 22251901]
18. Hetz C, Chevet E, & Harding HP (2013) Targeting the unfolded protein response in disease. Nature reviews. Drug discovery 12(9):703–719. [PubMed: 23989796]
19. Walter P & Ron D (2011) The unfolded protein response: from stress pathway to homeostatic regulation. Science 334(6059):1081–1086. [PubMed: 22116877]
20. Donnelly N, Gorman AM, Gupta S, & Samali A (2013) The eIF2alpha kinases: their structures and functions. Cellular and molecular life sciences : CMLS 70(19):3493–3511. [PubMed: 23354059]
21. Li Y, Guo Y, Tang J, Jiang J, & Chen Z (2014) New insights into the roles of CHOP- induced apoptosis in ER stress. Acta biochimica et biophysica Sinica 46(8):629–640. [PubMed: 25016584]

22. Bommiasamy H & Popko B (2011) Animal models in the study of the unfolded protein response. Methods in enzymology 491:91–109. [PubMed: 21329796]
23. Halliday M, Hughes D, & Mallucci GR (2017) Fine-tuning PERK signaling for neuroprotection. Journal of neurochemistry 142(6):812–826. [PubMed: 28643372]
24. Xiang C, Wang Y, Zhang H, & Han F (2017) The role of endoplasmic reticulum stress in neurodegenerative disease. Apoptosis 22(1):1–26. [PubMed: 27815720]
25. Wang L, Popko B, & Roos RP (2011) The unfolded protein response in familial amyotrophic lateral sclerosis. Human molecular genetics 20(5):1008–1015. [PubMed: 21159797]
26. Wang L, Popko B, & Roos RP (2014) An enhanced integrated stress response ameliorates mutant SOD1-induced ALS. Human molecular genetics.
27. Das I, et al. (2015) Preventing proteostasis diseases by selective inhibition of a phosphatase regulatory subunit. Science 348(6231):239–242. [PubMed: 25859045]
28. Jiang HQ, et al. (2014) Guanabenz delays the onset of disease symptoms, extends lifespan, improves motor performance and attenuates motor neuron loss in the SOD1 G93A mouse model of amyotrophic lateral sclerosis. Neuroscience 277:132–138. [PubMed: 24699224]
29. Wang L, Popko B, Tixier E, & Roos RP (2014) Guanabenz, which enhances the unfolded protein response, ameliorates mutant SOD1-induced amyotrophic lateral sclerosis. Neurobiology of disease 71:317–324. [PubMed: 25134731]
30. Vieira FG, et al. (2015) Guanabenz Treatment Accelerates Disease in a Mutant SOD1 Mouse Model of ALS. PloS one 10(8):e0135570. [PubMed: 26288094]
31. Vlug AS, et al. (2005) ATF3 expression precedes death of spinal motoneurons in amyotrophic lateral sclerosis-SOD1 transgenic mice and correlates with c-Jun phosphorylation, CHOP expression, somato-dendritic ubiquitination and Golgi fragmentation. The European journal of neuroscience 22(8):1881–1894. [PubMed: 16262628]
32. Harding HP, et al. (2001) Diabetes mellitus and exocrine pancreatic dysfunction in perk−/− mice reveals a role for translational control in secretory cell survival. Molecular cell 7(6):1153–1163. [PubMed: 11430819]
33. Vinsant S, et al. (2013) Characterization of early pathogenesis in the SOD1(G93A) mouse model of ALS: part II, results and discussion. Brain and behavior 3(4):431–457. [PubMed: 24381813]
34. Novoa I, Zeng H, Harding HP, & Ron D (2001) Feedback inhibition of the unfolded protein response by GADD34-mediated dephosphorylation of eIF2alpha. The Journal of cell biology 153(5):1011–1022. [PubMed: 11381086]
35. Lin W, et al. (2008) Enhanced integrated stress response promotes myelinating oligodendrocyte survival in response to interferon-gamma. The American journal of pathology 173(5):1508–1517. [PubMed: 18818381]
36. Novoa I, et al. (2003) Stress-induced gene expression requires programmed recovery from translational repression. The EMBO journal 22(5):1180–1187. [PubMed: 12606582]
37. Tsaytler P, Harding HP, Ron D, & Bertolotti A (2011) Selective inhibition of a regulatory subunit of protein phosphatase 1 restores proteostasis. Science 332(6025):91–94. [PubMed: 21385720]
38. Marciniak SJ, et al. (2004) CHOP induces death by promoting protein synthesis and oxidation in the stressed endoplasmic reticulum. Genes & development 18(24):3066–3077. [PubMed: 15601821]
39. Zinszner H, et al. (1998) CHOP is implicated in programmed cell death in response to impaired function of the endoplasmic reticulum. Genes & development 12(7):982–995. [PubMed: 9531536]
40. Engel T, et al. (2013) CHOP regulates the p53-MDM2 axis and is required for neuronal survival after seizures. Brain : a journal of neurology 136(Pt 2):577–592. [PubMed: 23361066]
41. Gow A & Wrabetz L (2009) CHOP and the endoplasmic reticulum stress response in myelinating glia. Current opinion in neurobiology 19(5):505–510. [PubMed: 19744850]
42. Gurney ME, et al. (1994) Motor neuron degeneration in mice that express a human Cu,Zn superoxide dismutase mutation. Science 264(5166):1772–1775. [PubMed: 8209258]
43. Bruijn LI, et al. (1997) ALS-linked SOD1 mutant G85R mediates damage to astrocytes and promotes rapidly progressive disease with SOD1-containing inclusions. Neuron 18(2):327–338. [PubMed: 9052802]

44. Acevedo-Arozena A, et al. (2011) A comprehensive assessment of the SOD1G93A low- copy transgenic mouse, which models human amyotrophic lateral sclerosis. Disease models & mechanisms 4(5):686–700. [PubMed: 21540242]
45. Philips T & Rothstein JD (2015) Rodent Models of Amyotrophic Lateral Sclerosis. Curr Protoc Pharmacol 69:5 67 61–21. [PubMed: 26344214]
46. Wong PC, et al. (1995) An adverse property of a familial ALS-linked SOD1 mutation causes motor neuron disease characterized by vacuolar degeneration of mitochondria. Neuron 14(6):1105–1116. [PubMed: 7605627]
47. Wang L, et al. (2009) Wild-type SOD1 overexpression accelerates disease onset of a G85R SOD1 mouse. Human molecular genetics 18(9):1642–1651. [PubMed: 19233858]
48. Rozas P, Bargsted L, Martinez F, Hetz C, & Medinas DB (2017) The ER proteostasis network in ALS: Determining the differential motoneuron vulnerability. Neurosci Lett 636:9–15. [PubMed: 27150076]
49. Matus S, Glimcher LH, & Hetz C (2011) Protein folding stress in neurodegenerative diseases: a glimpse into the ER. Current opinion in cell biology 23(2):239–252. [PubMed: 21288706]
50. Harding HP, Zhang Y, Bertolotti A, Zeng H, & Ron D (2000) Perk is essential for translational regulation and cell survival during the unfolded protein response. Molecular cell 5(5):897–904. [PubMed: 10882126]
51. Bertolotti A (2018) Importance of the subcellular location of protein deposits in neurodegenerative diseases. Current opinion in neurobiology 51:127–133. [PubMed: 29631171]
52. Sundaram JR, Lee IC, & Shenolikar S (2017) Translating protein phosphatase research into treatments for neurodegenerative diseases. Biochem Soc Trans 45(1):101–112. [PubMed: 28202663]
53. Rutkowski DT, et al. (2006) Adaptation to ER stress is mediated by differential stabilities of pro-survival and pro-apoptotic mRNAs and proteins. PLoS Biol 4(11):e374. [PubMed: 17090218]
54. Chatterjee J & Kohn M (2013) Targeting the untargetable: recent advances in the selective chemical modulation of protein phosphatase-1 activity. Curr Opin Chem Biol 17(3):361–368. [PubMed: 23647984]
55. Knight ZA & Shokat KM (2007) Chemical genetics: where genetics and pharmacology meet. Cell 128(3):425–430. [PubMed: 17289560]
56. Chen CM, Wu CT, Chiang CK, Liao BW, & Liu SH (2012) C/EBP homologous protein (CHOP) deficiency aggravates hippocampal cell apoptosis and impairs memory performance. PloS one 7(7):e40801. [PubMed: 22815824]
57. Huang H, et al. (2017) Neuroprotection by eIF2alpha-CHOP inhibition and XBP-1 activation in EAE/optic neuritiss. Cell death & disease 8(7):e2936. [PubMed: 28726788]
58. Silva RM, et al. (2005) CHOP/GADD153 is a mediator of apoptotic death in substantia nigra dopamine neurons in an in vivo neurotoxin model of parkinsonism. Journal of neurochemistry 95(4):974–986. [PubMed: 16135078]
59. Ohri SS, et al. (2011) Attenuating the endoplasmic reticulum stress response improves functional recovery after spinal cord injury. Glia 59(10):1489–1502. [PubMed: 21638341]
60. Alexander GM, et al. (2004) Effect of transgene copy number on survival in the G93A SOD1 transgenic mouse model of ALS. Brain research. Molecular brain research 130(1–2):7–15. [PubMed: 15519671]
61. Gurney ME (1997) The use of transgenic mouse models of amyotrophic lateral sclerosis in preclinical drug studies. Journal of the neurological sciences 152 Suppl 1:S67–73. [PubMed: 9419057]
62. Scott S, et al. (2008) Design, power, and interpretation of studies in the standard murine model of ALS. Amyotrophic lateral sclerosis : official publication of the World Federation of Neurology Research Group on Motor Neuron Diseases 9(1):4–15.
63. Kaja S, et al. (2007) Severely impaired neuromuscular synaptic transmission causes muscle weakness in the Cacna1a-mutant mouse rolling Nagoya. The European journal of neuroscience 25(7):2009–2020. [PubMed: 17439489]
64. Perez-Garcia MJ & Burden SJ (2012) Increasing MuSK activity delays denervation and improves motor function in ALS mice. Cell reports 2(3):497–502. [PubMed: 22939980]

65. Kennedy HS, Jones C 3rd, & Caplazi P (2013) Comparison of standard laminectomy with an optimized ejection method for the removal of spinal cords from rats and mice. J Histotechnol 36(3):86–91. [PubMed: 24039319]

Highlights

- The UPR is a cytoprotective pathway activated in response to ER stress.
- Genetic inhibition of UPR-PERK pathway had no effect on disease in mtSOD1 mice.
- Genetic enhancement of UPR-PERK pathway did not alleviate disease in mtSOD1 mice.
- Genetic ablation of pro-apoptotic *CHOP* did not alleviate disease in mtSOD1 mice.

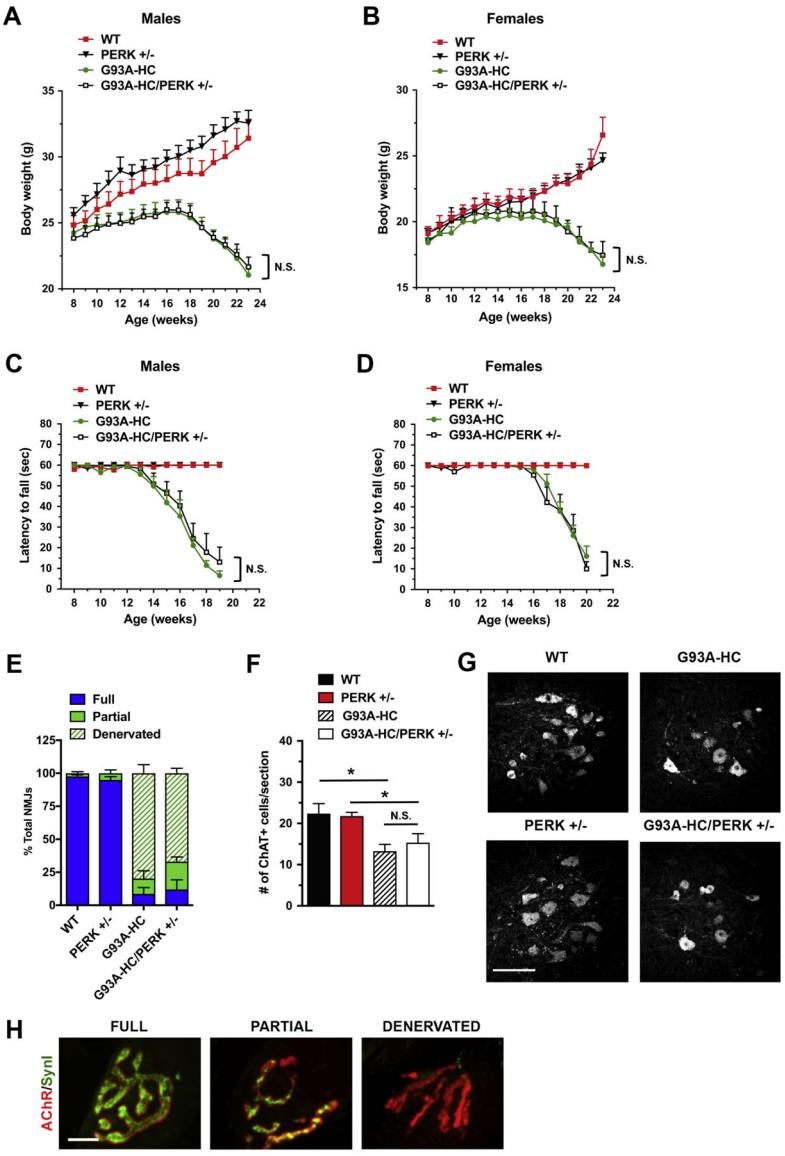

Figure 1. *PERK* deficiency does not affect disease in *G93A*-HC mice

(A, B) Body weights of male (A) and female (B) mice. No significant differences were found in *G93A*-HC/*PERK*$^{+/-}$ vs. *G93A*-HC mice (male or female). n = 6–7 males and n = 6–9 females per genotype. Two-way RM-ANOVA with Tukey's post hoc test. (C, D) Motor fatigue measurements of male (C) and female (D) mice using inverted grid-hanging test. The ability of *G93A*-HC mice to cling to the wire grid declined rapidly after 13 weeks of age for males, and after 15 weeks of age for females. *PERK* deficiency did not change the length of time *G93A*-HC mice cling to the grid. n = 6–7 males and n = 6–9 females per genotype. Two-way RM-ANOVA with Tukey's post hoc test. (E) Quantitation of tibialis anterior muscle innervation in early-symptomatic (15-week- old) mice. *PERK* deficiency had no effect on the extent of NMJ denervation in *G93A*-HC mice. n = 3 mice per genotype. % Fully innervated NMJs: 8.64% in *G93A*-HC vs. 11.95% in *G93A*- HC/*PERK*$^{+/-}$ P = 0.7264 (unpaired two-tailed t test). (F) Quantitation of ChAT-positive ventral horn motor neurons

(per lumbar spinal cord section) in 15-week-old animals revealed no significant difference between *G93A*-HC/*PERK*$^{+/-}$ and *G93A*-HC mice. $n = 3$ mice per genotype. One-way ANOVA with Tukey's post hoc test. (G) Representative images of ChAT-positive motor neurons in lumbar spinal cords of 15-week-old mice. Scale bar 100 μM. (H) Fully innervated, partially innervated, and denervated NMJs were distinguished by differences in co-localization of immunostaining for SynI (green) and AChRs (red). Scale bar 10 μM. Data are shown as mean ± SEM. *$P < 0.05$ N.S. = not significant.

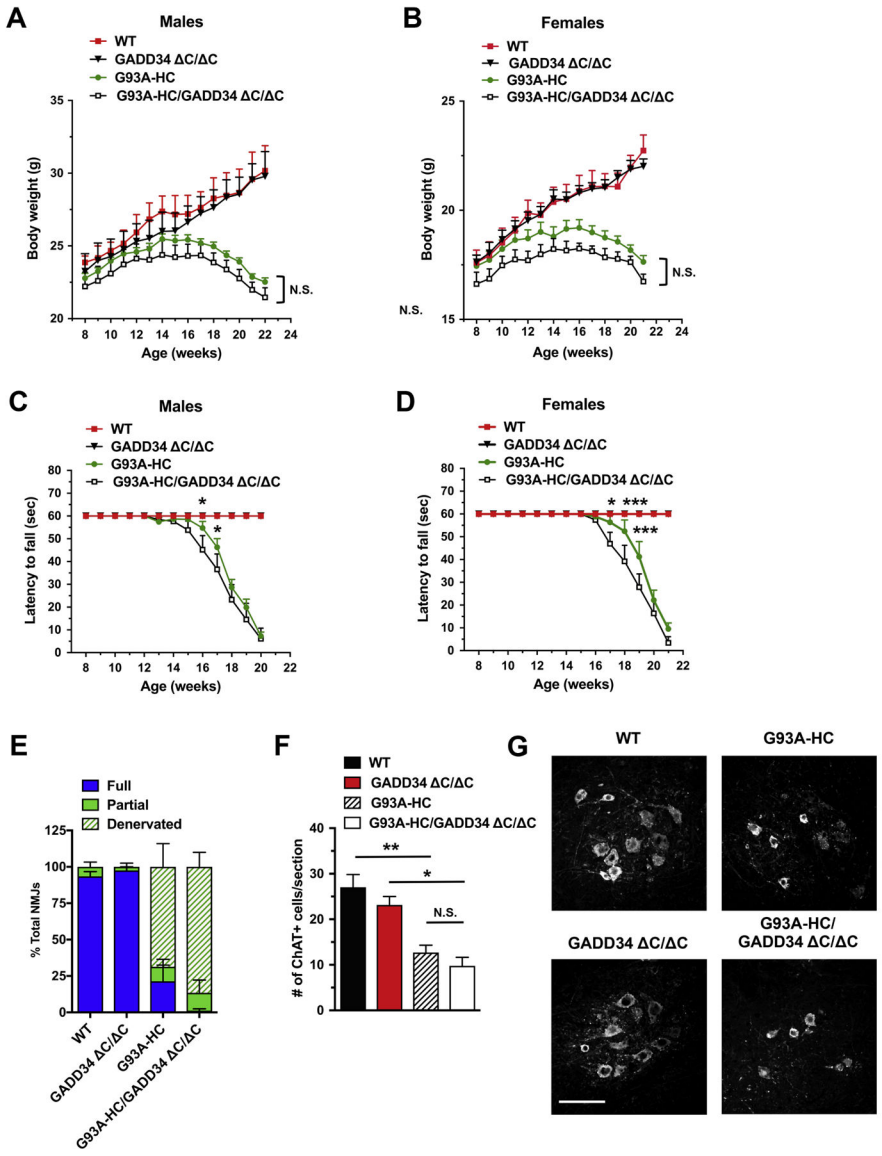

Figure 2. *GADD34* deficiency does not ameliorate disease in *G93A*-HC mice

(A, B) Body weights of male (A) and female (B) mice. No significant differences were found in *G93A*-HC/*GADD34*$^{\Delta C/\Delta C}$ vs. *G93A*-HC mice (male or female). $n = 6–9$ males and $n = 6–8$ females per genotype. Two-way RM-ANOVA with Tukey's post hoc test. (C, D) Motor fatigue measurements of male (C) and female (D) mice using inverted grid-hanging test. Male and female *G93A*-HC/*GADD34*$^{\Delta C/\Delta C}$ mice displayed significantly diminished latency to fall, compared to their age- and sex-matched *G93A*-HC littermates. $n = 6–9$ males and $n = 6–8$ females per genotype. Two-way RM-ANOVA with Tukey's post hoc test. (E) Quantitation of tibialis anterior muscle innervation in early-symptomatic (15-week-old) mice. *G93A*-HC/*GADD34*$^{\Delta C/\Delta C}$ mice displayed reduced NMJ innervation, although not statistically significant, compared to *G93A*-HC mice. $n = 3$ mice per genotype. % Fully innervated NMJs: 21.39% in *G93A*-HC vs. 1.23% in *G93A*-HC/*GADD34*$^{\Delta C/\Delta C}$ $P = 0.1447$ (unpaired two-tailed t test). (F) Quantitation of ChAT- positive ventral horn motor neurons

(per lumbar spinal cord section) in 15-week-old animals indicated that *GADD34* deficiency had no effect on motor neuron loss in *G93A*-HC mice. $n = 3$ mice per genotype. One-way ANOVA with Tukey's post hoc test. (G) Representative images of ChAT-positive motor neurons in lumbar spinal cords of 15-week-old mice. Scale bar 100 μM. Data are shown as mean ± SEM. $^{*}P < 0.05$ $^{**}P < 0.01$ $^{***}P < 0.001$ N.S. = not significant.

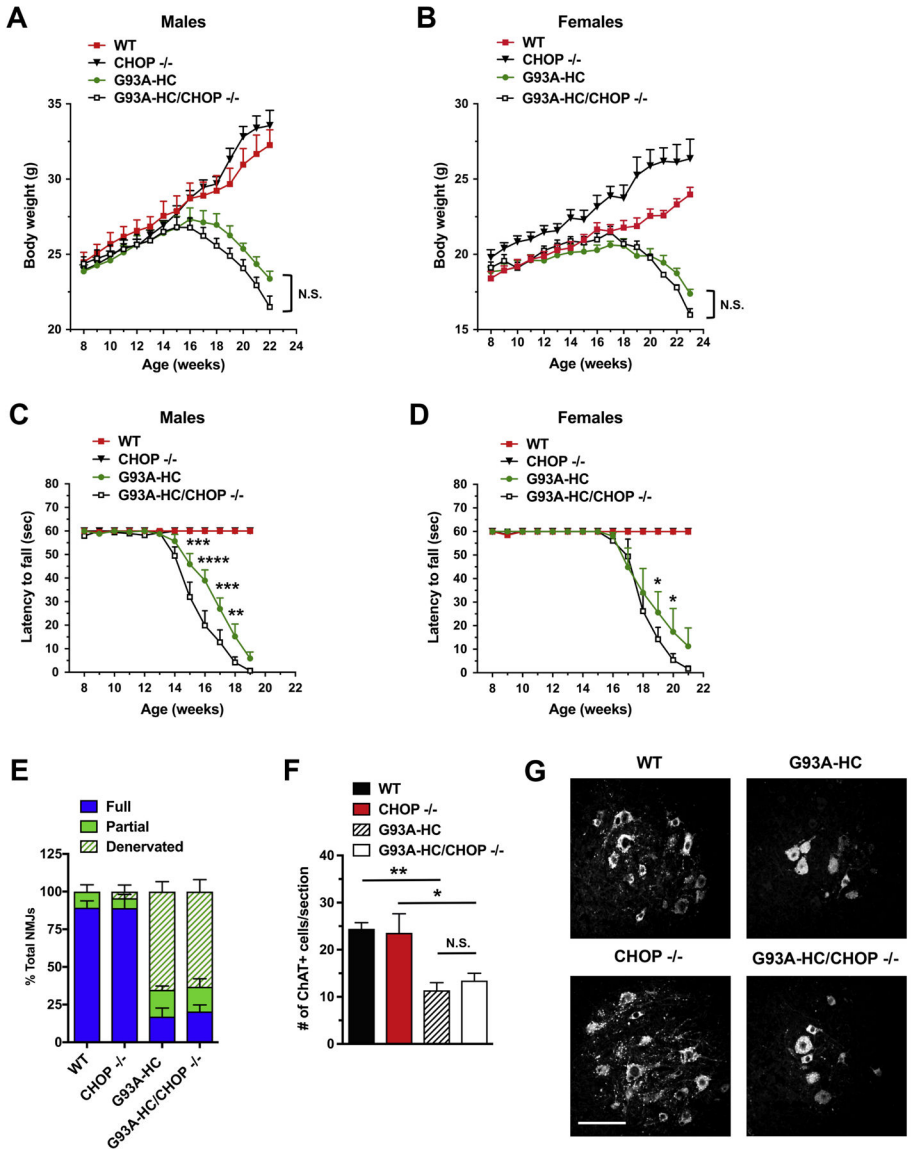

Figure 3. *CHOP* deficiency does not ameliorate disease in *G93A*-HC mice

(A, B) Body weights of male (A) and female (B) mice. No significant differences were found in *G93A*-HC/*CHOP*$^{-/-}$ vs. *G93A*-HC mice (male or female). n = 7–9 males and n = 6–9 females per genotype. Data are shown as mean ± SEM for each time point. Two-way RM-ANOVA with Tukey's post hoc test. (C, D) Motor fatigue measurements of male (C) and female (D) mice using inverted grid-hanging test. Male and female *G93A*-HC/*CHOP*$^{-/-}$ mice displayed significantly diminished latency to fall, compared to their age- and sex-matched *G93A*-HC littermates. n = 7–9 males and n = 6–9 females per genotype. Two-way RM-ANOVA with Tukey's post hoc test. (E) Quantitation of tibialis anterior muscle innervation in early-symptomatic (15- week-old) mice. *CHOP* deficiency had no effect on the extent of NMJ denervation in *G93A*-HC mice. n=3–4 mice per genotype. % Fully innervated NMJs: 17.08% in *G93A*-HC vs. 20.43% in *G93A*-HC/*CHOP*$^{-/-}$ P = 0.6565 (unpaired two-tailed t test). (F) Quantitation of ChAT-positive ventral horn motor neurons

(per lumbar spinal cord section) in 15-week-old animals indicated that *CHOP* deficiency had no effect on motor neuron loss in *G93A*-HC mice. n=3–4 mice per genotype. One-way ANOVA with Tukey's post hoc test. (G) Representative images of ChAT- positive motor neurons in lumbar spinal cords of 15-week-old mice. Scale bar 100 μM. Data are shown as mean ± SEM. $^{*}P < 0.05$ $^{**}P < 0.01$ $^{***}P < 0.001$ $^{****}P < 0.0001$ N.S. = not significant.

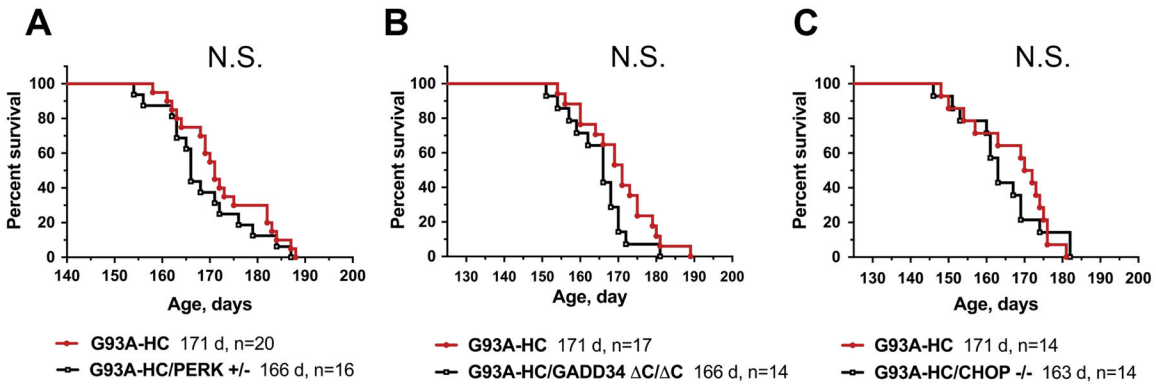

Figure 4. *PERK, GADD34,* and *CHOP* deficiencies do not affect survival in *G93A*-HC mice

No significant differences were found in the median survival times of *G93A*-HC mice deficient for *PERK* (A), *GADD34* (B), and *CHOP* (C) compared to their respective *G93A*-HC littermate controls. *n* = number of animals of the designated genotype. Log-rank (Mantel-Cox) test: *P* = 0.2636 (A), *P* = 0.2152 (B), *P* = 0.2391 (C). N.S. = not significant. Mice unable to right themselves within 20 s after being placed on their sides were defined as end-stage. This artificial endpoint was used to determine 'survival' reliably and humanely.

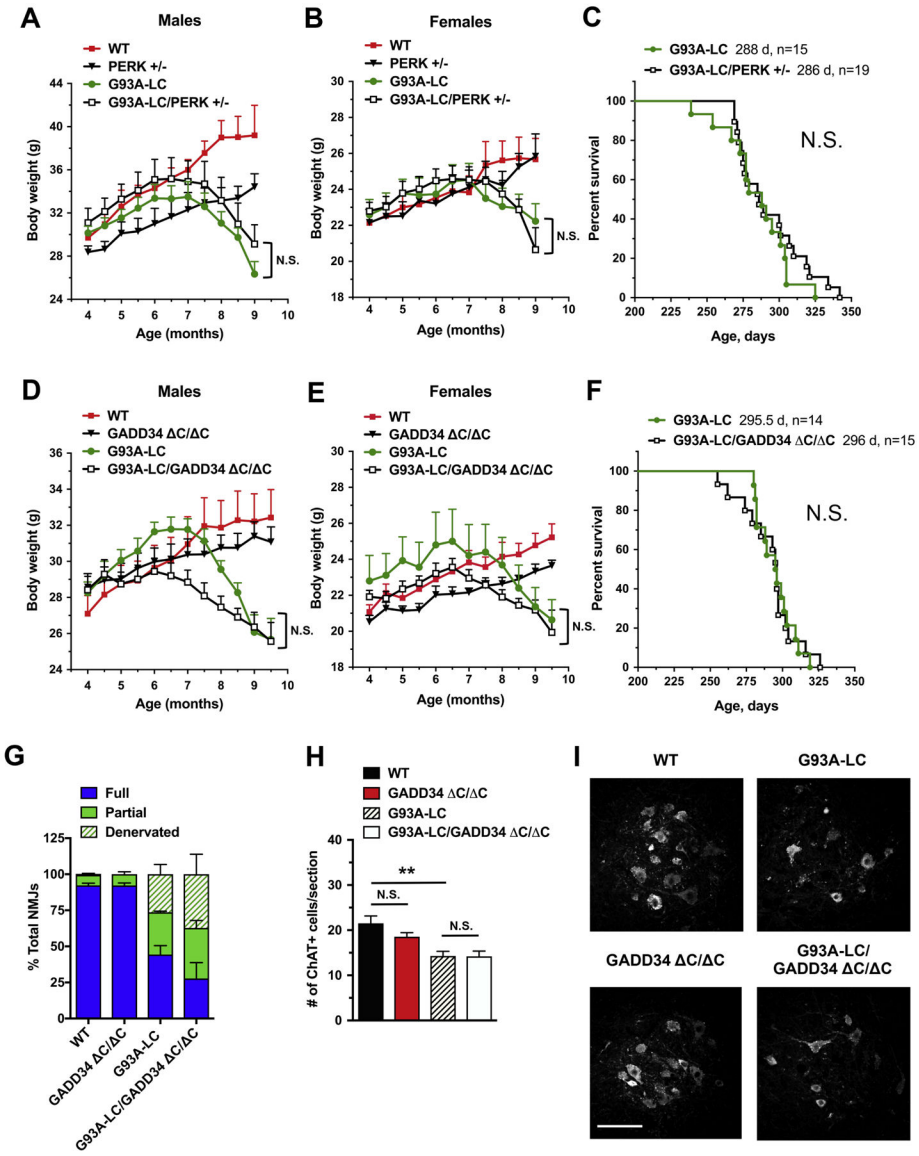

Figure 5. *PERK* and *GADD34* deficiencies do not affect disease in *G93A*-LC mice

(A, B, D, E) Body weights of male (A, D) and female (B, E) mice. No significant differences were found in *G93A*-LC/*PERK*$^{+/-}$ vs. *G93A*-LC mice (A, B) and in *G93A*-LC/*GADD34*$^{\Delta C/\Delta C}$ vs. *G93A*- LC mice (D, E). n = 6–10 males and n = 6–11 females per genotype. Two-way RM-ANOVA with Tukey's post hoc test. (C, F) There were no significant differences in the median survival times of *G93A*-LC/*PERK*$^{+/-}$ vs. *G93A*-LC mice (C) and in the median survival times of *G93A*- LC/*GADD34*$^{\Delta C/\Delta C}$ vs. *G93A*-LC mice (F). n = number of animals of the designated genotype. Log-rank (Mantel-Cox) test: P = 0.3601 (C), P = 0.9752 (F). N.S. = not significant. (G) Quantitation of tibialis anterior muscle innervation in early-symptomatic (8-month-old) animals demonstrated that *GADD34* deficiency had no significant effect on the extent of NMJ denervation in *G93A*-LC mice. n = 4 mice per genotype. % Fully innervated NMJs: 44.37% in *G93A*-LC vs. 27.83% in *G93A*-LC/*GADD34*$^{\Delta C/\Delta C}$ P = 0.2362 (unpaired two-tailed t test). (H) Quantitation of ChAT-

positive ventral horn motor neurons (per lumbar spinal cord section) in 8- month-old mice indicated that *GADD34* deficiency had no effect on motor neuron loss in *G93A*- LC mice. n = 4 mice per genotype. One-way ANOVA with Tukey's post hoc test. (G) Representative images of ChAT-positive motor neurons in lumbar spinal cords of 8-month-old mice. Scale bar 100 μM.

Data are shown as mean ± SEM. $^{**}P < 0.01$ N.S. = not significant.

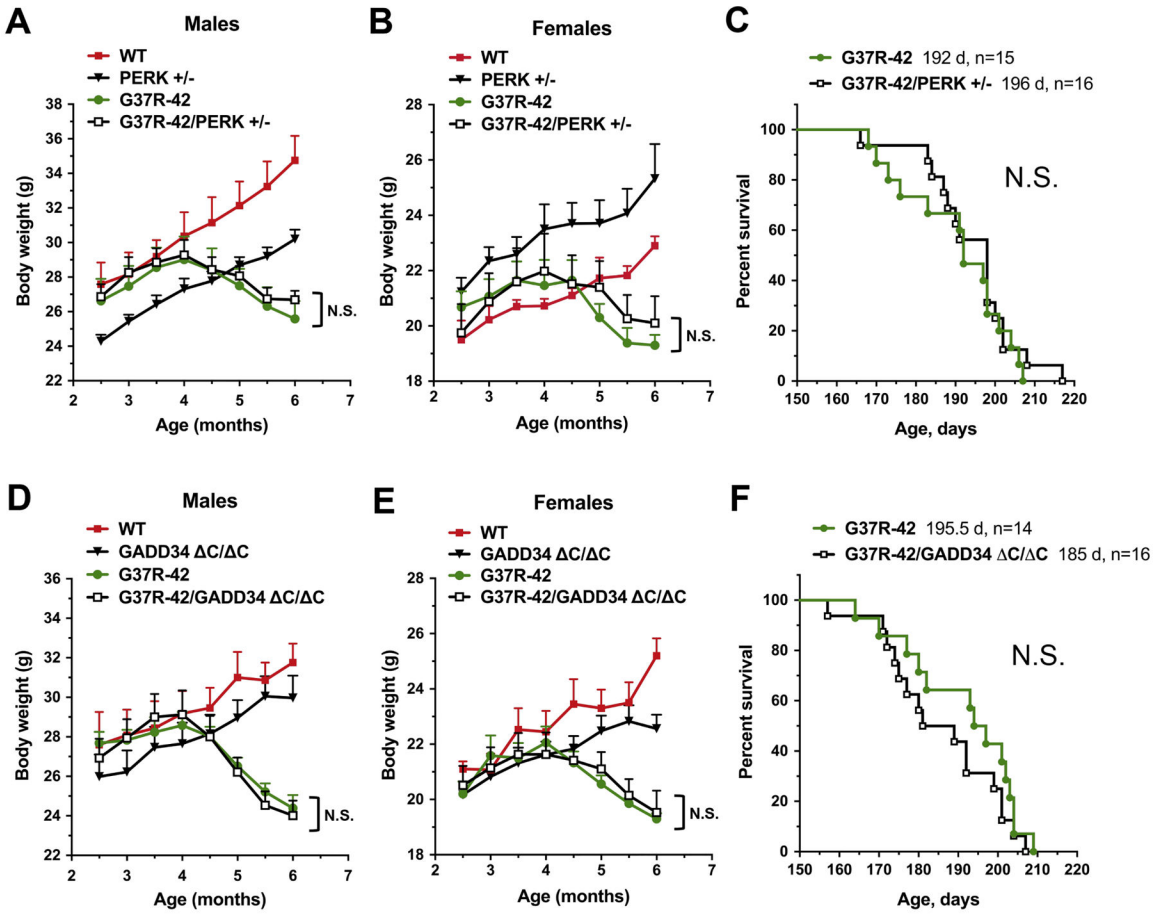

Figure 6. *PERK* and *GADD34* deficiencies do not affect disease in *G37R*-42 mice

(A, B, D, E) Body weights of male (A, D) and female (B, E) mice. No significant differences were found in *G37R*-42/*PERK*$^{+/-}$ vs. *G37R*-42 mice (A, B) and in *G37R*-42/*GADD34*$^{\Delta C/\Delta C}$ vs. *G37R*-42 mice (D, E). n = 6–9 males and n = 6–11 females per genotype. Two-way RM-ANOVA with Tukey's post hoc test. (C, F) There were no significant differences in the median survival times of *G37R*-42/*GADD34*$^{\Delta C/\Delta C}$ vs. *G37R-42* mice (C) and in the median survival times of *G37R*- 42/*GADD34*$^{\Delta C/\Delta C}$ vs. *G37R*-42 mice (F). n = number of animals of the designated genotype. Log- rank (Mantel-Cox) test: P = 0.4481 (C), P = 0.2383 (F). N.S.=not significant. Data are shown as mean ± SEM. N.S. = not significant.

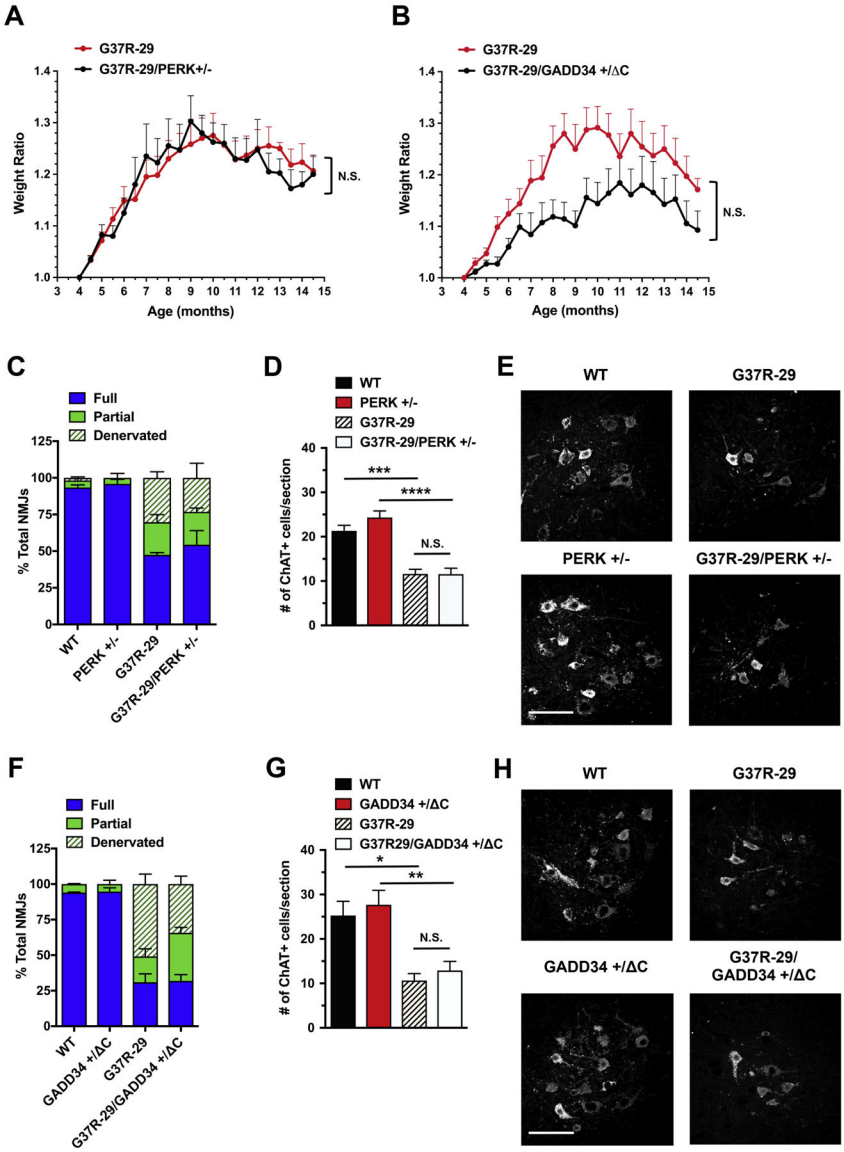

Figure 7. *PERK* and *GADD34* deficiencies do not affect disease in *G37R*-29 mice

(A, B) Body weight ratios were calculated relative to baseline weight measurement (in 4 month- old mice). No significant differences were found in weight trend of *G37R*-29/*PERK* $^{+/-}$ vs. *G37R*- 29 mice (A) and in weight trend of *G37R*-29/*GADD34*$^{+/\Delta C}$ vs. *G37R*-29 mice (B). Both male and female mice were used (n = 6–7 mice per genotype). Unpaired t test (one per time point) with Holm-Sidak correction for multiple comparisons. (C, F) Quantitation of tibialis anterior muscle innervation in early-symptomatic (14.5-month-old) mice demonstrated that *PERK* deficiency (C) and *GADD34* deficiency (F) had no effect on the extent of NMJ denervation in *G37R*-29 mice. n = 4 mice per genotype. % Fully innervated NMJs: 47.49% in *G37R*-29 vs. 54.41% in *G37R*- 29/*PERK*$^{+/-}$ P = 0.5028 (unpaired two-tailed t test) 30.94% in *G37R*-29 vs. 31.91% in *G37R*-29/*GADD34*$^{+/\Delta C}$ P = 0.8999 (unpaired two-tailed t test). (D, G) Quantitation of ChAT-positive ventral horn motor neurons (per lumbar spinal cord section) in 14.5-month-old mice indicated that *PERK*

deficiency (D) and *GADD34* deficiency (G) had no effect on motor neuron loss in *G37R*-29 mice. $n = 4$ mice per genotype. One-way ANOVA with Tukey's post hoc test. (E, H) Representative images of ChAT-positive motor neurons in lumbar spinal cords of 14.5-month-old mice with *PERK* deficiency (E) and *GADD34* deficiency (H). Scale bar 100 μM. Data are shown as mean ± SEM. $^{*}P < 0.05$ $^{**}P < 0.01$ $^{***}P < 0.001$ N.S. = not significant.

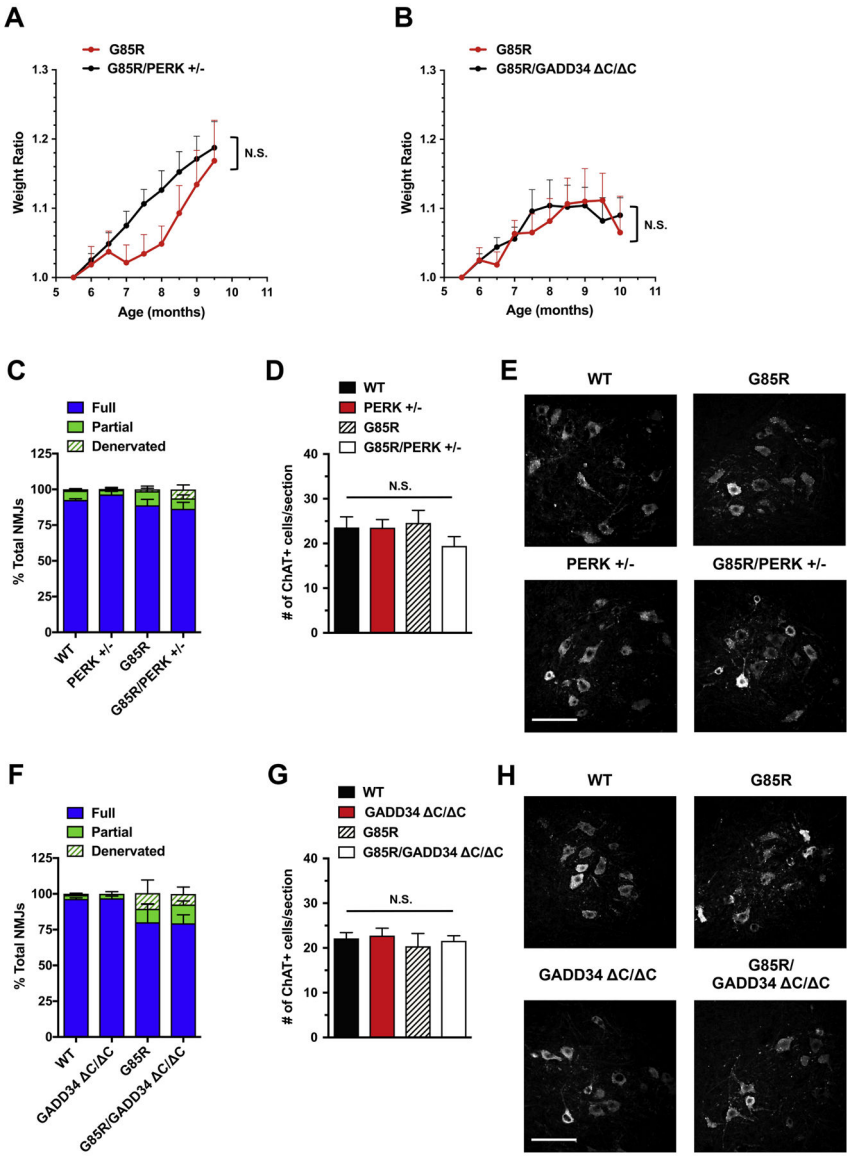

Figure 8. *PERK* and *GADD34* deficiencies do not affect disease in *G85R* mice

(A, B) Body weight ratios were calculated relative to baseline weight measurement (in 5.5 month-old mice). No significant differences were found in weight trend of *G85R*/*PERK*$^{+/-}$ vs. *G85R* mice (A) and in weight trend of *G85R*/*GADD34*$^{\Delta C/\Delta C}$ vs. *G85R* mice (B). Both male and female mice were used (n = 6–8 mice per genotype). Unpaired t test (one per time point) with Holm-Sidak correction for multiple comparisons. (C, F) Quantitation of tibialis anterior muscle innervation demonstrated that *PERK* deficiency (C) did not exacerbate NMJ innervation in 9.5- month-old mice (time point corresponding to disease onset in *G85R* controls). n = 4 mice per genotype. % Fully innervated NMJs: 88.87% in *G85R* vs. 86.49% in *G85R*/*PERK*$^{+/-}$ P = 0.7121 (unpaired two-tailed t test). As expected from precipitous disease course in *G85R* mice, NMJ innervation in these 9.5-month-old mice was comparable to that in WT controls. (F) *GADD34* deficiency had no effect on the extent of NMJ denervation in early-diseased (10-month-old) *G85R* mice. n = 4 mice per genotype. % Fully

innervated NMJs: 80.22% in *G85R* vs. 79.43% in *G85R*/*GADD34*$^{\Delta C/\Delta C}$ $P = 0.9568$ (unpaired two-tailed *t* test). (D, G) Quantitation of ChAT-positive ventral horn motor neurons (per lumbar spinal cord section) indicated that *PERK* deficiency (D) and *GADD34* deficiency (G) had no effect on motor neuron numbers in *G85R* mice. $n = 4$ mice per genotype. One-way ANOVA with Tukey's post hoc test. As expected from the disease course in *G85R* mice, motor neuron numbers in these mice were normal at 9.5–10 months of age. (E, H) Representative images of ChAT-positive motor neurons in lumbar spinal cords of *G85R* mice with *PERK* deficiency (E) and *GADD34* deficiency (H). Scale bar 100 μM. Data are shown as mean ± SEM. N.S.=not significant.

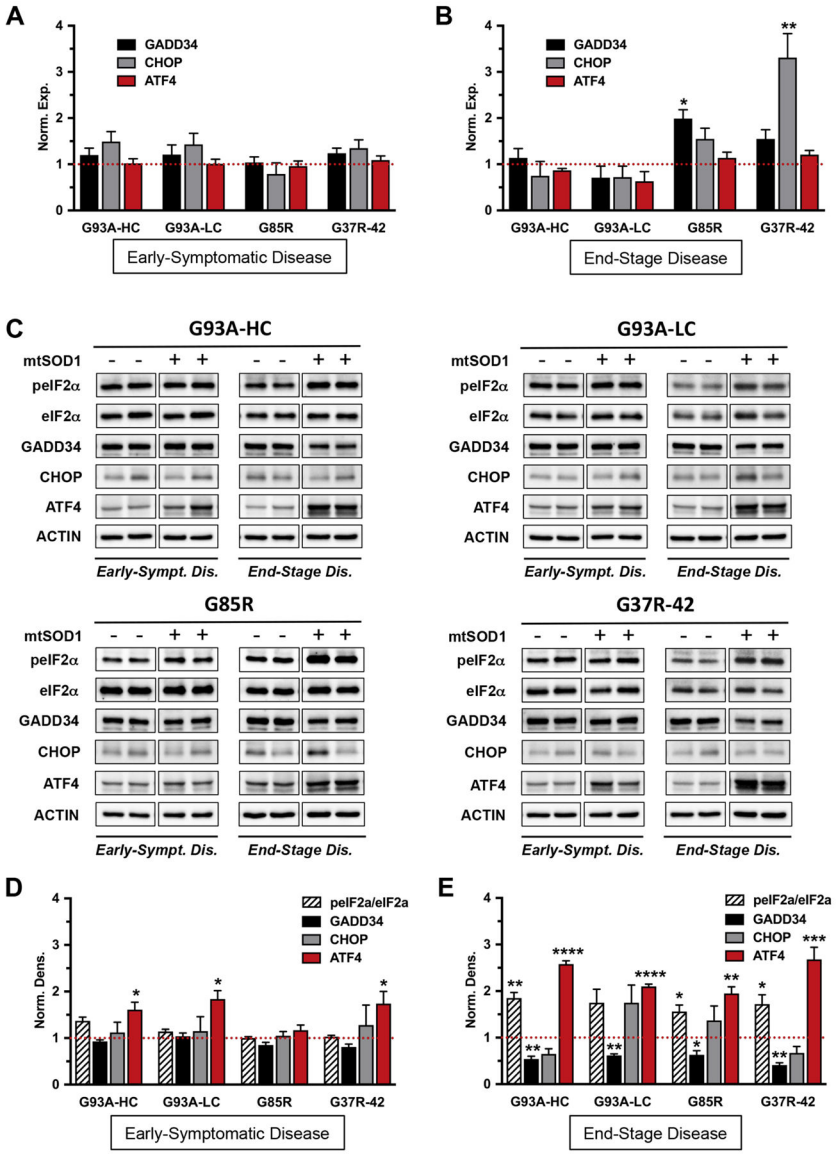

Figure 9. Biochemical analyses of the PERK pathway in spinal cords of early- symptomatic and end-stage mutant SOD1 mice.

The PERK pathway activation is not detected in spinal cords of early-symptomatic mtSOD1 mice. Moreover, increased eIF2α phosphorylation in spinal cords of end-stage mtSOD1 mice does not induce downstream UPR components CHOP and GADD34. (A, B) Real-time qPCR for *GADD34*, *CHOP* and *ATF4* mRNA levels in lumbar spinal cords from mtSOD1 mice with early-symptomatic disease (A) and end-stage disease (B). Data were normalized to actin reference gene and expressed as mean ± SEM fold change relative to age-matched WT controls (red dashed line). $n = 4$ mice per group. Norm. exp. = normalized expression. (C) Representative immunoblots of p-eIF2α (phosphorylated), eIF2α, GADD34, CHOP, and ATF4 protein levels in lumbar spinal cords from mtSOD1 mice with early-symptomatic and end-stage disease, and their age-matched WT controls. Actin was used as a loading control. (D, E) Quantification of p-eIF2α/eIF2α, GADD34, CHOP, and ATF4 protein levels in lumbar spinal cords from mtSOD1 mice with early-symptomatic disease (D) and end-

stage disease (E). Data were normalized to actin and expressed as mean ± SEM fold change relative to age-matched WT controls (red dashed line). $n = 3–4$ mice per group. Norm. dens. = normalized densitometry. Unpaired t test: $^{*}P < 0.05$ $^{**}P < 0.01$ $^{***}P < 0.001$ $^{****}P < 0.0001$.

Table 1.

Lines of transgenic mice expressing human SOD1 mutation

hSOD1 Mutation	Dismutase Activity	Disease Onset (Age)	Early-Symptomatic Disease (Symptoms, Age)	End-Stage Disease/Survival (Age)
G93A-high copy	Active	~4 months	Hind limb tremors with tail suspension, ~4 months	~6 months
G93A-low copy	Active	~6.5 months	Hind limb tremors with tail suspension, ~8 months	~10 months
G85R	Inactive	~9.5 months	No obvious tremors, mild weight loss, ~10 months	~11 months
G37R-42	Active	~4 months	Hind limb tremors with tail suspension, ~4.5 months	~6.5 months
G37R-29	Active	~10 months	Hind limb tremors with tail suspension, ~14.5 months	~17 months

hSOD1=human superoxide dismutase 1. Disease onset was defined as peak body weight before a decline. Early-symptomatic disease was defined by the appearance of first clinical symptoms. End-stage disease was defined by the inability of a mouse with limb paralysis to right itself within 20 s after being placed on its side. This artificial endpoint is universally used to determine ‘survival’ reliably and humanely. Disease onset, early-symptomatic disease, and end-stage/survival time points were determined experimentally for each mouse line. For immunohistochemical and biochemical analyses, tissues were collected from mice with early-symptomatic and end-stage disease at time points as indicated.